

Prepared for:

Rijkswaterstaat

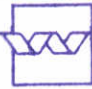

Dienst Weg- en Waterbouwkunde, TAW-A1

SKYLLA: Wave motion in and on coastal structures

Implementation of impermeable slopes and
overtopping-boundary conditions

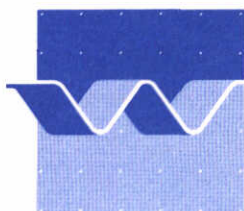
AFGEHANDELD

Oktober 1994

	bibliotheek postbus 177 - 2800 MH Delft waterloopkundig laboratorium/WL
BB	62950 / 62946 / 63876
WL	VERVALLEN
EXPL	 R0002370

SKYLLA: Wave motion in and on coastal structures

Implementation of impermeable slopes and
overtopping-boundary conditions



delft hydraulics

1. Report no. H1780.11	2. Serial no. TAW-A1	3. Catalog no. addressee	
4. Title and sub-tittle SKYLLA: Wave motion in and on coastal structures. Implementation of impermeable slopes and overtopping-boundary conditions.		5. Report date October 1994	
		6. Code H1780	
7. Author(s) H.A.H. Petit, P. van den Bosch, M.R.A. van Gent		8. Report no.	
9. Name and address Waterloopkundig Laboratorium Voorsterweg 28, Marknesse Postbus 152 8300 AD Emmeloord		10. Project name TAWA*BELAST	
		11. Contract reference DWW-745	
12. Name and address principal Rijkswaterstaat Dienst Weg- en Waterbouwkunde Postbus 5044 2600 GA Delft		13. Report status FINAL	
		14. Code of other principal	
15. Remarks This report has been made in cooperation with the Delft University of Technology, Hydraulic Engineering Division			
16. Summary Wave motion on an in coastal structures can be simulated with the numerical program SKYLLA. The model has been extended with several types of internal boundary conditions which allow the modelling of impermeable structures with both climbing and falling slopes.			
17. Keywords Wave motion, impermeable structures		18. Distribution system	
19. Classification Accessible	20. Classification this page	21. Number of pages	22. Cost

Contents

List of symbols

	page
1 Introduction	1
1.1 Framework for the development of the model SKYLLA	1
1.2 Considerations for the development of the model SKYLLA	1
1.3 Description of the numerical model SKYLLA	2
1.4 Required program modifications	2
1.5 Outline	3
2 Implementation of the free-slip boundary conditions	4
2.1 Mathematical and physical description of the free-slip boundary conditions	4
2.2 Numerical implementation of the free-slip boundary conditions	4
2.3 Adapting a user-supplied polygon	9
2.4 Tests with impermeable structures	12
2.5 Overtopping-boundary conditions and applicability	21
2.6 Numerical implementation	22
2.7 Tests with overtopping-boundary conditions	25
2.8 Unresolved problems at sharp edges	32
3 Conclusions and recommendations	34

References

- Appendices:**
- A - Numerical treatment of falling and climbing slopes in SKYLLA**
 - B - Suggested approach for releasing a jet of water at an edge on the slope**
 - C - Stability considerations**
 - D - Average-prescribing weakly-reflective boundary conditions**

List of symbols

a	coefficient in Forchheimer terms	(s/m)
b	coefficient in Forchheimer terms	(s ² /m ²)
c	wave celerity	(m/s)
C_M	coefficient in Forchheimer terms	(-)
F	fraction of cell filled with fluid	(-)
g	gravitational acceleration	(m/s ²)
g_x	x-components of gravitational acceleration vector	(m/s ²)
g_y	y-components of gravitational acceleration vector	(m/s ²)
h	mean water depth	(m)
i, j	indexes indicating the location of the cell	(-)
n	porosity	(-)
n	coordinate in normal direction	(m)
p	pressure	(N/m ²)
P	reduced pressure ($P=p/\rho_w$)	(m ² /s ²)
t	time	(s)
u	velocity vector	(m/s)
u	x-component of velocity vector	(m/s)
u_n	normal velocity component at a slope	(m/s)
u_τ	tangential velocity component at a slope	(m/s)
v	y-component of velocity vector	(m/s)
x	coordinate in horizontal direction	(m)
y	coordinate in vertical direction	(m)
α	upwind fraction in discretizations	(-)
ρ_w	density of water	(kg/m ³)
Δx_i	distance between vertical grid lines with indexes i and $i-1$	(m)
Δy_j	distance between horizontal grid lines with indexes j and $j-1$	(m)
τ	coordinate in tangential direction	(m)

1 Introduction

1.1 Framework for the development of the model SKYLLA

The development of the numerical model SKYLLA began within the framework of the European research project "MAST-G6 Coastal Structures". The aim was to develop a physical-based numerical formulation for water motion on a smooth slope and also on-and-in permeable structures. This formulation lead to the numerical model SKYLLA¹. Due to the inspiring results obtained in this European project, The Road and Hydraulic Division (Rijkswaterstaat) of the Dutch Ministry of Transport and Public Works was prepared to lead the continuation of the development (see contracts DWW 743 and DWW 745). This further development, outside the European MAST-project, started in 1993.

The research comprised the following tasks:

- 1) Boundary conditions, (Petit et al. 1993)
- 2) Rubble mound structures and porous flow, (van Gent et al. 1993)
- 3) Downward slopes and overtopping, (this report)
- 4) Treatment of turbulence,
- 5) Treatment of air-entrapment,
- 6) Treatment of roughness.

The planning of those tasks is described in detail in (Klein Breteler and Petit, 1993). This report describes the research dealing with Task 2.

1.2 Considerations for the development of SKYLLA

Numerous coastal structures are studied using small-scale physical models. Physical modelling can be influenced by scale effects, due to which various phenomena can be different under prototype conditions compared to conditions present in small-scale physical models. These problems, as well as the complexity of measurements in breaking waves, can be overcome by numerical modelling of breaking waves on-and-in coastal structures. So, on the one hand the development of a numerical model as a research tool is very important; on the other there are disadvantages such as the simplification and discretization of the involved physical processes.

Existing one-dimensional models use simplified formulations of, for example, the free surface. For many applications these simplifications are undesirable. The development of a three-dimensional model able to simulate the complete breaking of waves within the near future, seems unrealistic. Therefore, it was decided to develop a two-dimensional (vertical) numerical model that can simulate breaking waves on various types of coastal structures, first for wave motion on smooth impermeable slopes and, at a later stage, for wave motion on-and-in permeable structures. A proper representation of the wave impact will not yet be included.

¹ The model SKYLLA is named after the sea monster from the Greek mythology, being a mistress of Poseidon and living on a rock eating shipwrecked sailors.

1.3 Description of the numerical model SKYLLA

The studies performed within the European MAST-project resulted in the research tool SKYLLA, which is able to simulate breaking waves on impermeable smooth slopes. These studies are described in (Broekens and Petit, 1992) and in (Petit and Van den Bosch, 1992) and are summarized by (Van der Meer et al., 1992). A brief summary is given below.

The model solves the two-dimensional Navier-Stokes equations in two dimensions with a constant turbulence viscosity. The technique for solving these equations is based on the "Volume of Fluid method" (VOF), see (Nichols and Hirt, 1980). The fluid is considered incompressible. The model uses a staggered, non-equidistant grid where for each cell the fluid fraction can vary between zero (empty) and one (full)(Eulerian approach).

The model uses a complex description of the free surface based on an adapted flux-method known as "FLAIR", see (Ashgriz and Poo, 1991) and is capable of simulating free surfaces that can become multiple-connected, while air-entrapment can be dealt with. Those two aspects are essential for the simulation of plunging waves. The entrapped air is modelled as if it were vacuum.

The model includes the option to model a smooth impermeable climbing slope with a 'free-slip' boundary condition. The choice of the grid is independent of the lay out of the slope.

In the previous phases of the development of SKYLLA, incident waves as prescribed by (Rienecker and Fenton, 1981) were implemented. Both the left-hand side boundary and the right-hand side boundary can be made weakly reflective, enabling waves to leave the computational domain with an acceptably small disturbance of the wave motion in the computational domain.

Furthermore, in SKYLLA the option was introduced to model flow through porous material, thus allowing the modelling of structures that are permeable or contain permeable parts.

For both the flow on and in a porous structure and for the flow on an impermeable structure, numerical results were compared with measurements to validate the program; see (Van Gent et al., 1993) and (Van Gent et al., 1994).

1.4 Required program modifications

The result of the European MAST project was a description of the numerical method to model an impermeable climbing slope in a VOF solver. The numerical formulations for both 'free-slip' and 'no-slip' boundary conditions were examined. The new boundary conditions for the 'free-slip' case were implemented in the SKYLLA code. Results of the numerical work were presented in (Petit and Van den Bosch, 1992).

The limitation to climbing slopes was found to be too great a limitation for the possible applications of SKYLLA. Overtopping a dike, submerged impermeable structures, a toe of a structure, and structures with a berm reservoir, are examples of cases where the option of modelling a falling slope in SKYLLA is required.

In the case where overtopping is to be modelled and where the velocities at the top of the structure can be assumed supercritical the computation can be done in two steps. The first

computation is used to simulate the process in a domain which contains the top of the structure but not far beyond. The second computation uses the results of the first which were recorded as a time signal on a vertical line which is located at the top of the structure. This location is the inflow boundary of the second model where the flow of the water which overtopped is simulated. Both the recording of the relevant data as time signals and the use of these signals as input for SKYLLA had to be implemented.

The implementation of falling slopes and overtopping boundary conditions will be described in this report.

1.5 Outline

The physical and short numerical description of the free-slip boundary conditions, a description of overtopping boundary conditions, and tests for the implemented program extensions are given in Chapter 2. Conclusions and recommendations are given in Chapter 3.

In appendix A an extensive description is given of the free-slip boundary conditions for all cell categories which can be used to model a slope.

Appendix B describes a possible solution for shortcomings of the implemented boundary conditions.

Better stability conditions which were implemented in SKYLLA are derived in Appendix C. Improved weakly reflective boundary conditions are discussed in Appendix D.

2 Implementation of free-slip boundary conditions

2.1 Mathematical and physical description of the free-slip boundary conditions

Flow parallel to a solid wall causes a boundary layer as the water on the solid wall cannot move relative to the wall. Internal friction in the water will tend to slow down the fluid particles near the boundary. If the velocity at some distance from the boundary is oscillating, the boundary layer cannot fully develop and the region where the effect of the boundary is felt remains relatively small. If the generation of turbulence energy at the boundary and the loss of this energy are not modelled the free-slip boundary condition is a good approximation of the effect of the boundary on the flow at some distance from the boundary. What it does is disregarding altogether the velocity reduction caused by the boundary.

As in this approximation there is no wall friction, the velocity component which is parallel to the boundary does not vary locally in the direction perpendicular to the boundary. As the boundary is impermeable the normal component of the velocity is zero at the boundary. These conditions can be expressed by:

$$\frac{\partial u_{\tau}}{\partial n} = 0 \text{ and } u_n = 0 \text{ at the boundary}$$

Here u_{τ} is the velocity component parallel to the boundary, u_n is the component perpendicular to the boundary and n is the local coordinate perpendicular to the boundary.

2.2 Numerical implementation of the free-slip boundary conditions

In (Petit & van den Bosch, 1992) a description of how the free-slip boundary conditions can be implemented, is given for the four cell categories that can be used to model a climbing slope.

Here ten new cell categories are introduced to enable a more flexible definition of the impermeable structure. Within the boundaries of a cell the impermeable surface of the structure is approximated by a straight line.

For each of the 14 cell categories an example is given in Figure 1.

Here we see that we also allow for horizontal and vertical parts in the structure to be modelled.

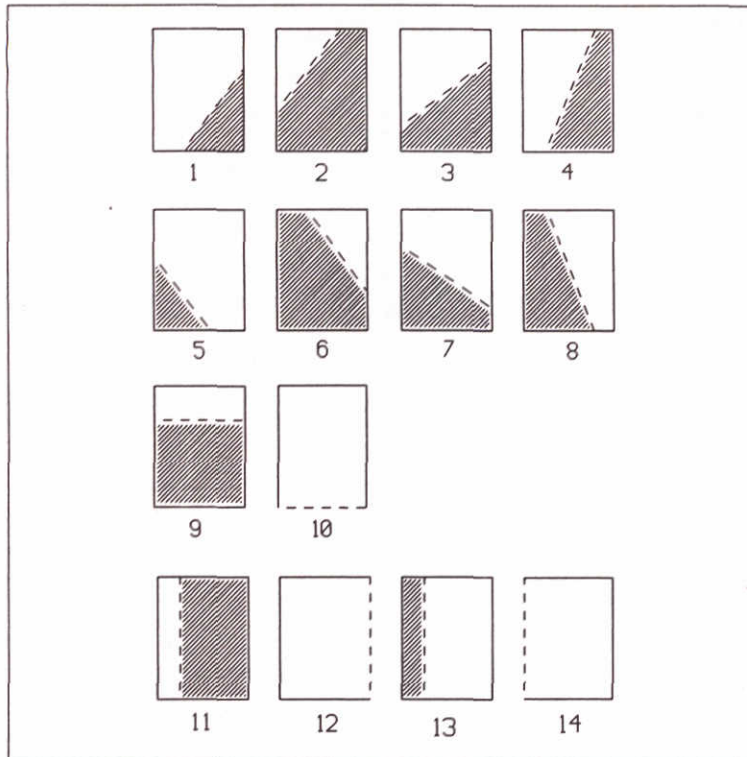


Figure 1 Examples of the 14 impermeable-boundary cell categories

In Appendix A a detailed description is given of the discretization of the free-slip boundary conditions for each of the 14 cell categories. The discretizations allow the combination of an impermeable boundary and an isotropic porous medium. The case when the boundary cell also contains a part of the free surface needs special attention. For these cases a discretization of the Navier-Stokes equations is not possible. The boundary conditions for the pressure at the slope can therefore not be based on physics. Here we chose the boundary conditions such that stability of the numerical treatment would be guaranteed.

In this section we will give a derivation of the numerical treatment for a cell of category 7. Here we assume that the free surface is not in the proximity of the boundary cell.

In the general case when porous material is included the modified Navier-Stokes equations are, see (Van Gent, Petit & van den Bosch, 1993) and (Van Gent, 1991):

$$\frac{\partial u}{\partial t} + \frac{n}{1+C_M} \frac{\partial}{\partial x} \left(\frac{u^2}{n} \right) + \frac{n}{1+C_M} \frac{\partial}{\partial y} \left(\frac{u v}{n} \right) = - \frac{n}{(1+C_M)\rho_w} \frac{\partial p}{\partial x} + \frac{n}{1+C_M} v_t \nabla^2 u - g \frac{n}{1+C_M} (au + bu|u|) + \frac{n}{1+C_M} g_x \quad (1)$$

$$\frac{\partial v}{\partial t} + \frac{n}{1+C_M} \frac{\partial}{\partial x} \left(\frac{u v}{n} \right) + \frac{\partial}{\partial y} \left(\frac{v^2}{n} \right) = - \frac{n}{(1+C_M)\rho_w} \frac{\partial p}{\partial y} + \frac{n}{1+C_M} v_t \nabla^2 v - g \frac{n}{1+C_M} (av + bv|u|) + \frac{n}{1+C_M} g_y \quad (2)$$

$$\frac{\partial u}{\partial x} + \frac{\partial v}{\partial y} = 0 \quad (3)$$

where

- u : filter velocity in x-direction (m/s)
- v : filter velocity in y-direction (m/s)
- n : porosity (-)
- ρ_w : specific density of water (kg/m³)
- p : pressure (N/m²)
- a : dimensional coefficient (s/m)
- b : dimensional coefficient (s²/m²)
- C_M : coefficient for "added mass" ($\gamma(1-n)/n$)
- g_x : gravitational acceleration in x direction (m/s²)
- g_y : gravitational acceleration in y-direction (m/s²)
- g : modulus of the gravitational acceleration (m/s²)

For the discretization we introduce:

$$n_{i+\frac{1}{2},j} = \frac{\Delta x_i n_{i+1,j} + \Delta x_{i+1} n_{ij}}{\Delta x_i + \Delta x_{i+1}}$$

$$n_{ij+\frac{1}{2}} = \frac{\Delta y_j n_{ij+1} + \Delta y_{j+1} n_{ij}}{\Delta y_j + \Delta y_{j+1}}$$

$$\gamma_{ij} = \frac{n_{i+\frac{1}{2},j}}{1 + C_M(n_{i+\frac{1}{2},j})}$$

$$\lambda_{ij} = \frac{n_{ij+\frac{1}{2}}}{1 + C_M(n_{ij+\frac{1}{2}})}$$

We discretize the reduced pressure $P_{ij} = \frac{p_{ij}}{\rho_w}$

Note that in the absence of porous material ($n=1$) the modified Navier-Stokes equations reduce to the well-known N-S equations.

In Figure 2 we show a cell of category 7 and several x- and y-velocity components in the staggered arrangement used in SKYLLA. The velocity components indicated by the dotted lines (and a name with an overbar) are the so-called 'virtual velocities'. These velocities do not represent real flow but are merely introduced to satisfy both boundary conditions at the collocation point indicated by the small circle.

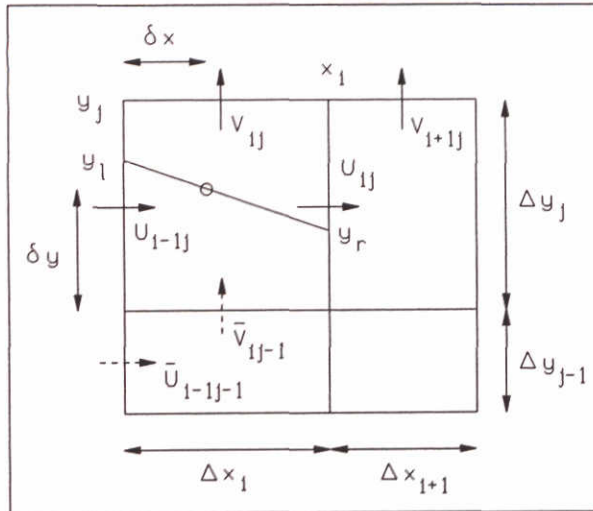


Figure 2 Boundary cell of category 7

We introduce the normal and the tangential unit vectors at the impermeable slope \mathbf{n} and $\boldsymbol{\tau}$ with x - and y components indicated by the subindex 1 and 2 respectively.

In order to find the velocity components u and v at the collocation point at the slope we use a linear approximation:

$$u = u_{ij} - (\Delta x_i - \delta x) \frac{\partial u}{\partial x} + (\delta y - \frac{1}{2} \Delta y_j) \frac{\partial u}{\partial y}$$

and

$$v = v_{ij} - (\Delta y_j - \delta y) \frac{\partial v}{\partial y} - (\frac{1}{2} \Delta x_i - \delta x) \frac{\partial v}{\partial x}$$

The partial derivatives in these expressions are approximated by:

$$\frac{\partial u}{\partial x} \approx \frac{u_{ij} - u_{i-1j}}{\Delta x_i}, \quad \frac{\partial u}{\partial y} \approx \frac{u_{i-1j} - \bar{u}_{i-1j-1}}{\frac{1}{2}(\Delta y_j + \Delta y_{j-1})}, \quad \frac{\partial v}{\partial x} \approx \frac{v_{i+1j} - v_{ij}}{\frac{1}{2}(\Delta x_i + \Delta x_{i+1})} \text{ and}$$

$$\frac{\partial v}{\partial y} \approx \frac{v_{ij} - \bar{v}_{ij-1}}{\Delta y_j}$$

Using the relations above, the impermeability condition $\mathbf{u}_n = \mathbf{u} \cdot \mathbf{n} = 0$ can now be approximated by:

$$\begin{aligned} n_1 [u_{ij} - (\Delta x_i - \delta x) \frac{u_{ij} - u_{i-1j}}{\Delta x_i} + 2(\delta y - \frac{1}{2} \Delta y_j) \frac{u_{i-1j} - \bar{u}_{i-1j-1}}{\Delta y_j + \Delta y_{j-1}}] + \\ + n_2 [v_{ij} - (\Delta y_j - \delta y) \frac{v_{ij} - \bar{v}_{ij-1}}{\Delta y_j} + 2(\delta x - \frac{1}{2} \Delta x_i) \frac{v_{i+1j} - v_{ij}}{\Delta x_{i+1} + \Delta x_i}] = 0 \end{aligned} \quad (4)$$

The zero shear-stress condition $\frac{\partial u_\tau}{\partial n} = 0$ can be approximated by:

$$\begin{aligned}\frac{\partial u_\tau}{\partial n} &= \mathbf{n} \cdot \nabla(\mathbf{u} \cdot \boldsymbol{\tau}) \approx n_1 \frac{\partial}{\partial x}(u \tau_1 + v \tau_2) + n_2 \frac{\partial}{\partial y}(u \tau_1 + v \tau_2) \\ &\approx n_1 \tau_1 \frac{\partial u}{\partial x} + n_1 \tau_2 \frac{\partial v}{\partial x} + n_2 \tau_1 \frac{\partial u}{\partial y} + n_2 \tau_2 \frac{\partial v}{\partial y} \\ &= n_1 \tau_1 \left(\frac{\partial u}{\partial x} - \frac{\partial v}{\partial y} \right) + n_1 \tau_2 \frac{\partial v}{\partial x} + n_2 \tau_1 \frac{\partial u}{\partial y} = 0\end{aligned}$$

By again using the relations above we find:

$$n_1 \tau_1 \left(\frac{u_{ij} - u_{i-1j}}{\Delta x_i} - \frac{v_{ij} - v_{ij-1}}{\Delta y_j} \right) + 2n_1 \tau_2 \frac{v_{i+1j} - v_{ij}}{\Delta x_{i+1} + \Delta x_i} + 2n_2 \tau_1 \frac{u_{i-1j} - u_{i-1j-1}}{\Delta y_j + \Delta y_{j-1}} = 0 \quad (5)$$

Equations (4) and (5) form a linear set of equations for the unknown virtual velocities \bar{u}_{i-1j-1} and \bar{v}_{ij-1} .

The mass conservation equation for this cell is an approximation of:

$$\oint_{\partial w} \mathbf{u} \cdot \mathbf{n} \, dl$$

where the integral is determined over ∂w which is the boundary of the quadrilateral part of the cell that can contain fluid.

The discretization now becomes:

$$(y_j - y_r) u_{ij}^{n+1} - (y_j - y_l) u_{i-1j}^{n+1} + \Delta x_i v_{ij}^{n+1} = 0$$

The pressure boundary condition can be derived from this by substituting:

$$\begin{aligned}v_{ij}^{n+1} &= \tilde{v}_{ij} - 2 \Delta t \lambda_{ij} \frac{P_{ij+1}^{n+1} - P_{ij}^{n+1}}{\Delta y_j + \Delta y_{j+1}}, \quad u_{ij}^{n+1} = \tilde{u}_{ij} - 2 \Delta t \gamma_{ij} \frac{P_{i+1j}^{n+1} - P_{ij}^{n+1}}{\Delta x_i + \Delta x_{i+1}} \text{ and} \\ u_{i-1j}^{n+1} &= \tilde{u}_{i-1j} - 2 \Delta t \gamma_{i-1j} \frac{P_{ij}^{n+1} - P_{i-1j}^{n+1}}{\Delta x_{i-1} + \Delta x_i}\end{aligned}$$

we find

$$\begin{aligned}& \frac{2 \Delta t (y_j - y_r)}{\Delta x_{i+1} + \Delta x_i} \gamma_{ij} (P_{i+1j}^{n+1} - P_{ij}^{n+1}) - \frac{2 \Delta t (y_j - y_l)}{\Delta x_i + \Delta x_{i-1}} \gamma_{i-1j} (P_{ij}^{n+1} - P_{i-1j}^{n+1}) + \\ & + \frac{2 \Delta t \Delta x_i}{\Delta y_{j+1} + \Delta y_j} \lambda_{ij} (P_{ij+1}^{n+1} - P_{ij}^{n+1}) = (y_j - y_r) \tilde{u}_{ij} - (y_j - y_l) \tilde{u}_{i-1j} + \Delta x_i \tilde{v}_{ij}\end{aligned} \quad (6)$$

The 'tilde' velocities represent the result of a part of the discretization of the Equations (1) and (2) (see van Gent, Petit & van den Bosch, App.A, 1993).

2.3 Adapting a user-supplied polygon

Since there are only 14 cell categories that can be used to model a slope in SKYLLA, a general user-supplied polygon cannot directly be used to describe the surface of the impermeable structure. An example of where things go wrong inside a cell is given in Figure 3. Here we see that within the cell the slope is not modelled as a single straight line. A second example is given in Figure 4 where the line inside the cell is straight but there is also a part of the polygon which coincides with the cell boundary. In appendix A all cell categories and special cases which can be dealt with in SKYLLA are given.

In order to avoid that a user of the program has to model a slope by defining all cell intersections, SKYLLA can adapt a user-supplied polygon to fit the requirements. Here we will give a brief description of the method used for that purpose.

When a polygon is supplied by the user the following steps are followed.

By traversing the polygon from knot to knot it is first checked if the polygon has more than one knot per cell. If so, the excess number of knots is removed from this cell, thereby changing the polygon.

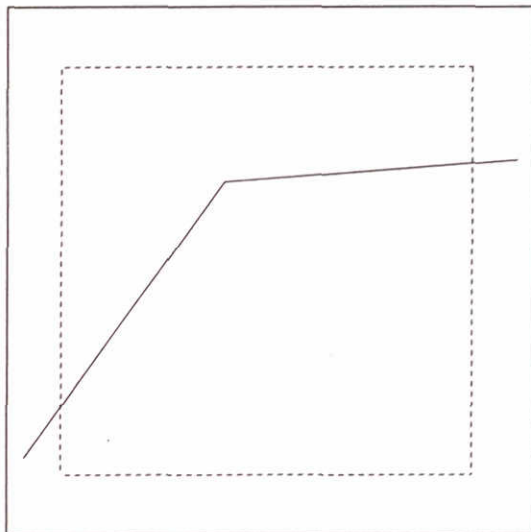


Figure 3 Angle inside cell

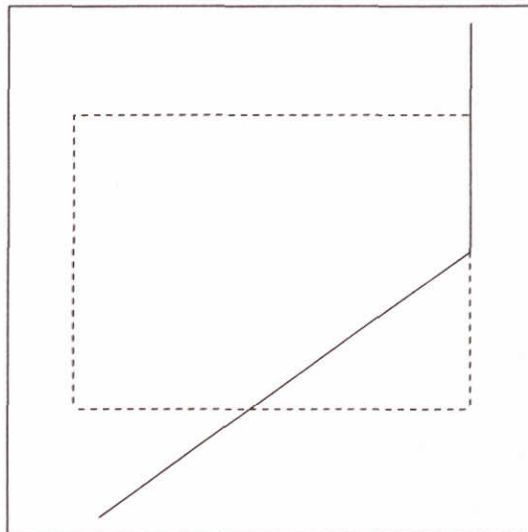


Figure 4 Part of boundary on edge

In the second step each of the remaining knots in the polygon is replaced by a new knot which is the projection on the nearest grid line. The polygon thus created may still not satisfy all the requirements as is shown by the example in Figure 5.

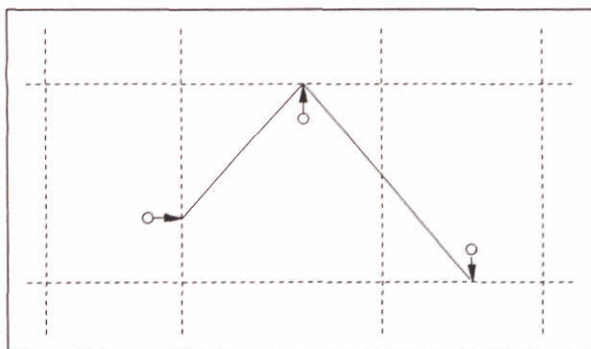


Figure 5 Non-existing cell category

In Appendix A a list is given of the possible categories of the neighbours of a cell of a given category. In the following we will schematically show how the polygon is changed (by the subroutine SLPCTR) in those cases where problems still occur.

Note that in many of these cases new knots are introduced.

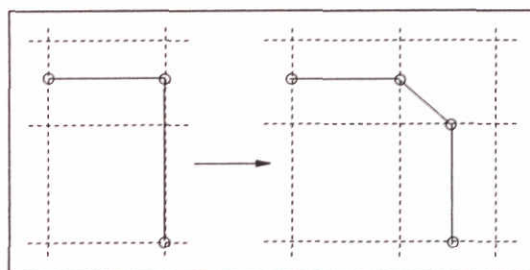


Figure 6 Horizontal to vertical

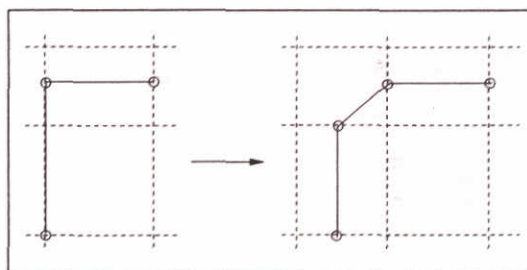


Figure 7 Vertical to horizontal

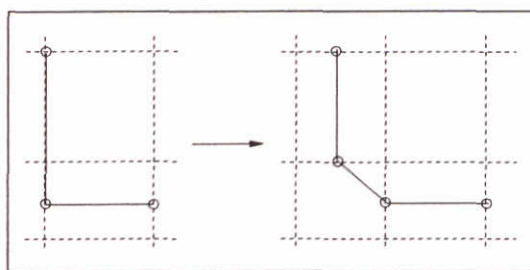


Figure 8 Vertical to horizontal

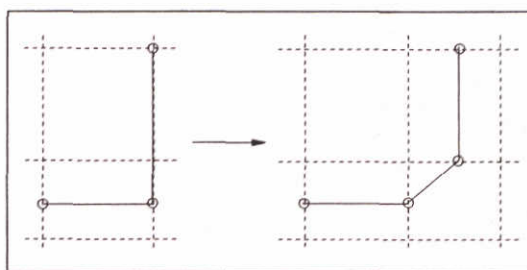


Figure 9 Horizontal to vertical

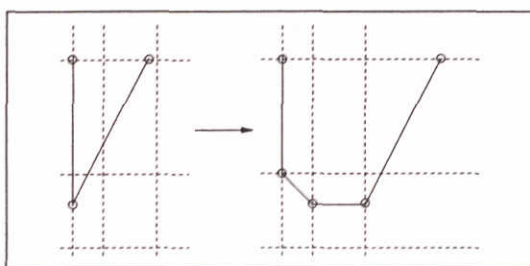


Figure 10 Vertical to climbing

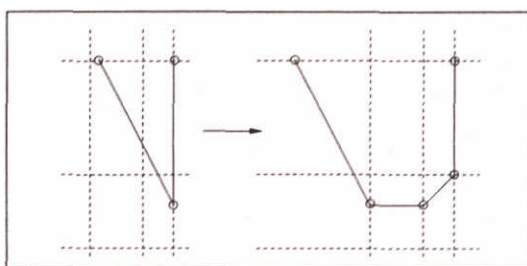


Figure 11 Falling to vertical

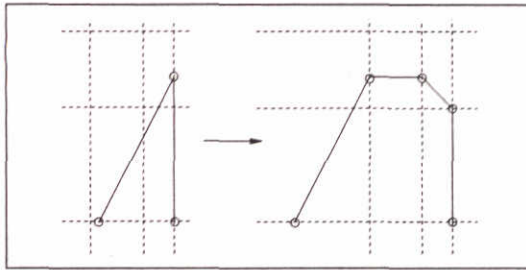


Figure 12 Climbing to vertical

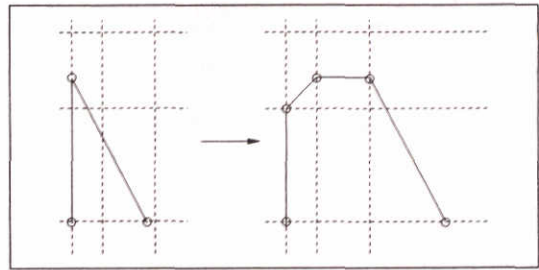


Figure 13 Vertical to falling

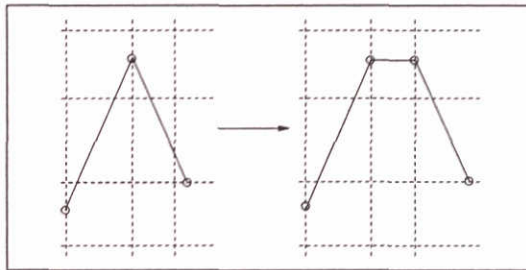


Figure 14 Climbing to falling

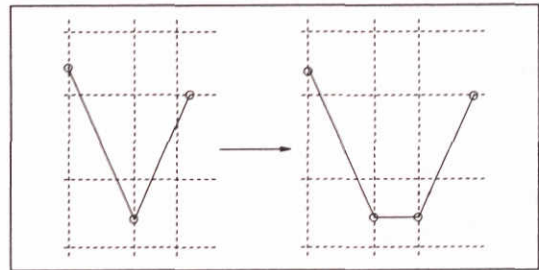


Figure 15 Falling to climbing

In the following cases no new knots are introduced.

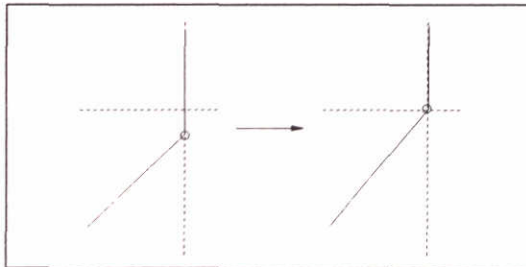


Figure 16 Climbing to vertical

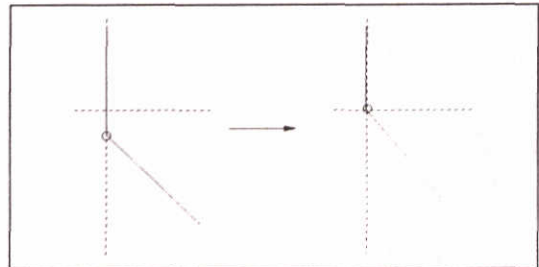


Figure 17 Vertical to falling

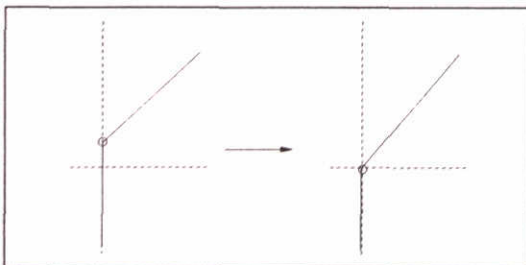


Figure 18 Vertical to climbing

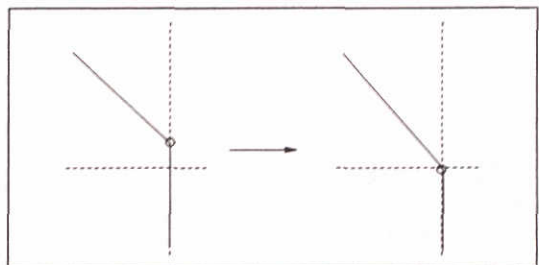


Figure 19 Falling to vertical

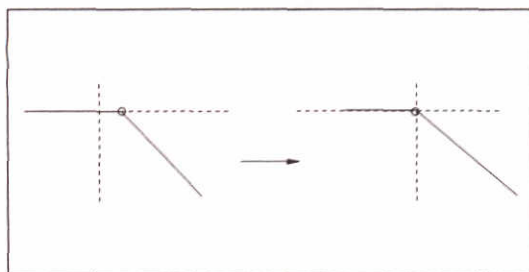


Figure 19a Horizontal to falling

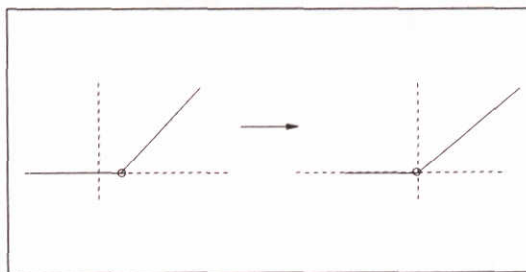


Figure 19b Horizontal to climbing

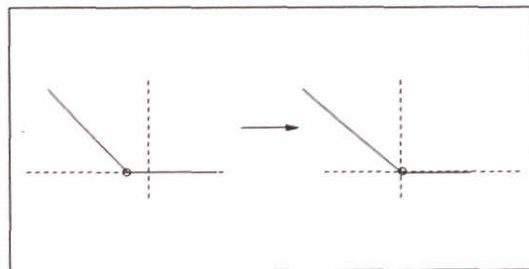


Figure 19c Falling to horizontal

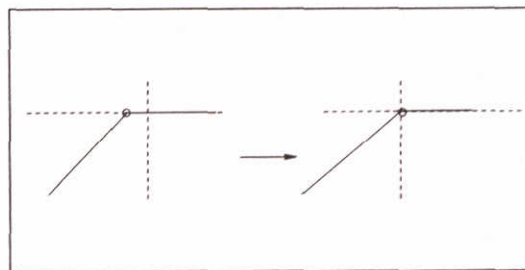


Figure 19d Climbing to horizontal

2.4 Tests with impermeable structures

In the following we shall show the results of tests with impermeable structures.

In the first four tests we show that for a slope with both falling and climbing parts the numerically implemented boundary conditions work well.

Figure 20 shows a symmetrical structure and the resulting velocity field of the flow computations.

In Figures 21 and 22 the left and the right parts of this symmetrical structure are shown.

Going from left to right along the slope in Fig. 21 we encounter cells of category:

3, 3, 3, 2, 2, 12, 12, 3, 3, 3, 3, 3, 3, 2, 10, and 10

respectively.

The fifth boundary cell (on the interval $1.4 < x < 1.5$) was generated by the program because a cell containing a climbing slope as well as a vertical part does not fall into one of the categories. The slope in this cell is modelled as a diagonal (category 2) as is shown in Figure 20a.

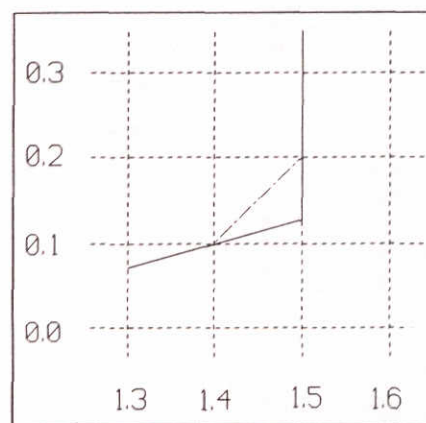


Figure 20a Adjusted slope

The polygon shown in Figure 21 is the polygon supplied by the user.

Again going from left to right in Figure 22 we encounter the cells of category:

10, 10, 6, 7, 7, 7, 7, 7, 7, 14, 14, 6, 6, 7, 7, and 7

respectively.

The thirteenth cell was again generated by the program because the configuration as given by the user for the cell in the interval $4.5 < x < 4.6$ cannot be modelled using the 14 cell categories we use. The program replaces the given configuration by a cell with a diagonal slope.

The components of the velocity vectors shown in Figures 21 and 22 were determined by averaging the horizontal and vertical velocity components which were determined at the cell boundaries. The result is a velocity vector at the centre of each cell. Virtual velocity components were also used to determine this vector plot. As can be seen in Figure 21 and 22 this also results in velocity vectors inside the structure.

Near the surface of the structure we see that velocity has no component normal to the slope. This shows that the impermeability condition is numerically satisfied. Furthermore, we see that at the slope the tangential component hardly changes in the direction normal to the slope indicating that the implemented free-slip condition is also satisfied.

In Figures 23 and 24 we see the same slopes (climbing and falling) as in the last test. In this test, however, we reduced the cell size in the vertical direction by a factor 1/2.

The lists of cell categories encountered by going from left to right along the slope are for Figures 23 and 24 respectively:

3, 2, 3, 2, 3, 12, 12, 12, 12, 12, 3, 3, 3, 3, 3, 3, 2, 1, 2, 10, 10

and

10, 10, 6, 5, 6, 7, 7, 7, 7, 7, 7, 14, 14, 14, 14, 14, 6, 6, 7, 6, 7.

Again we see that the boundary conditions are satisfied. Near the edge of the vertical part just above the gently sloping part of the slope, however, we find that the vertical component of the velocity is too large.

Figures 25 and 26 which show the result of a computation where the flow along the same slope was modelled using cells in which the vertical size was reduced by a factor 1/4. The same effect can be seen here near the edge of the vertical part of the slope. It is caused by the fact that the virtual velocity at the bottom of the boundary cell at the edge was determined by the free-slip condition at the vertical part.

In the Figures 27 and 28 we show the results of a computation with a slightly changed slope in order to introduce cells of categories 4 and 8.

The cell categories in this test are for Figures 27 and 28 respectively:

2, 2, 2, 2, 2, 12, 12, 12, 12, 12, 12, 12, 12, 12, 12, 3, 3, 3, 3, 3, 2, 4, 4, 4,
1, 2, 4, 4, 4, 1, 2, 4, 4, 4, 10, 10

and

10, 10, 8, 8, 8, 6, 5, 8, 8, 8, 6, 5, 8, 8, 8, 6, 7, 7, 7, 7, 7, 14, 14, 14, 14, 14,
14, 14, 14, 14, 14, 14, 6, 6, 6, 6, 6

We see that the virtual velocities introduced by the cells of category 4 (Figure 27, $2.0 < x < 2.3$) are relatively large in this case. However inside the wet domain they look fine. In Figure 28 the same happens for cells of category 8 ($3.7 < x < 4.0$).

In Figures 29 to 36 we show snapshots of a computation with waves on a low crested berm. Figure 29 shows the initial still-water condition. Figures 30 and 31 show how the incoming wave runs up and overtops the left part of the structure, runs down the falling part of the structure and runs up on the second climbing part. The rest of the figures show the backwash which fills up the canal on the structure and starts running down the left climbing slope where it meets the second incoming wave which reverses the direction of the flow.

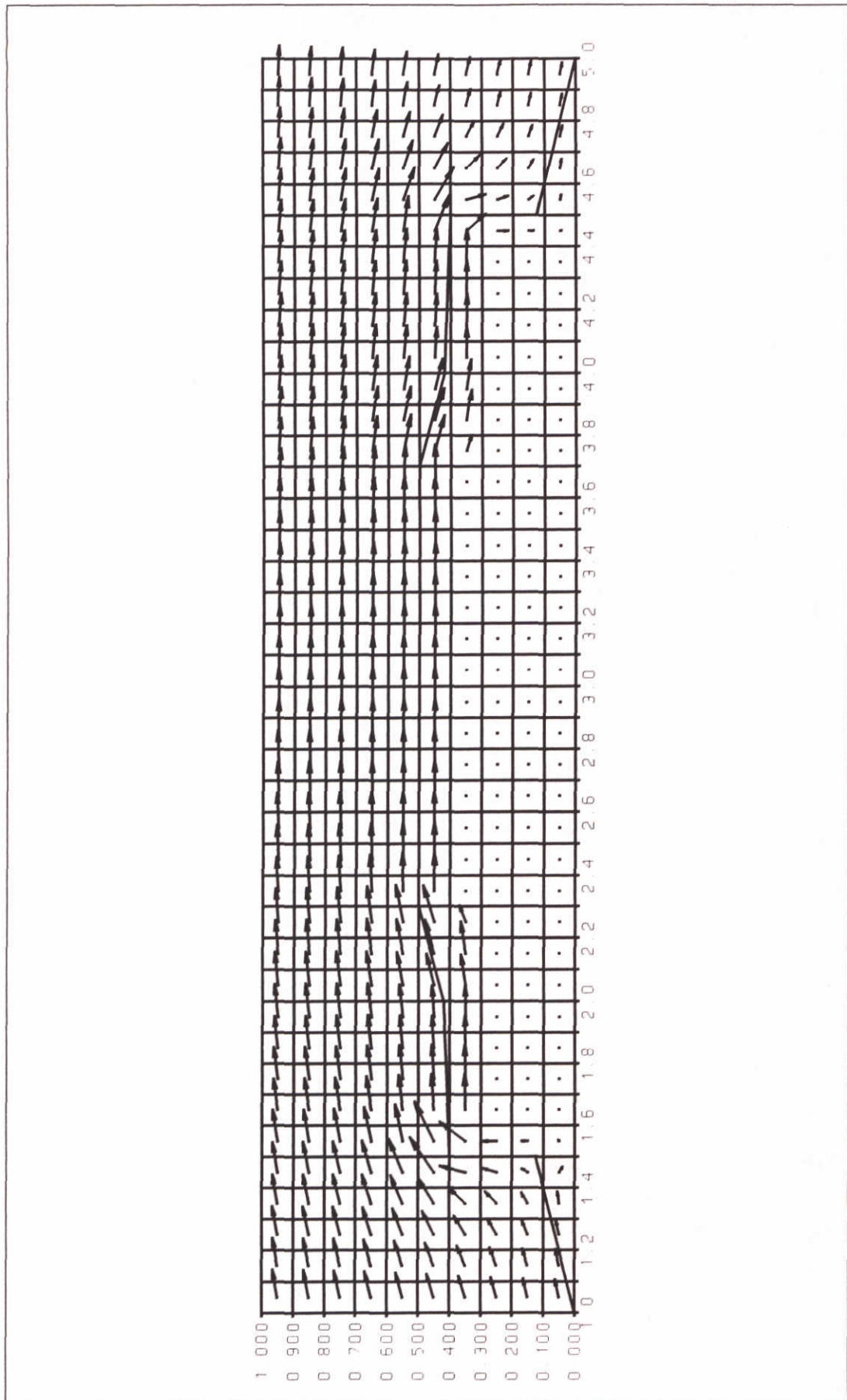


Figure 20 General layout of test

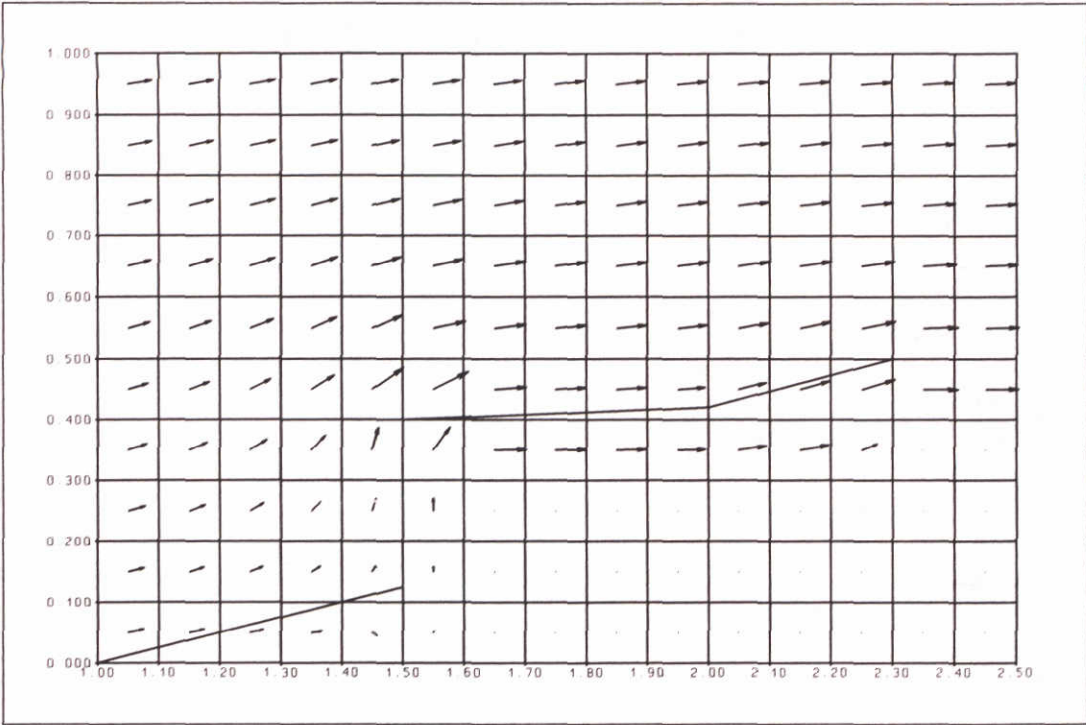


Figure 21 Left part of the structure

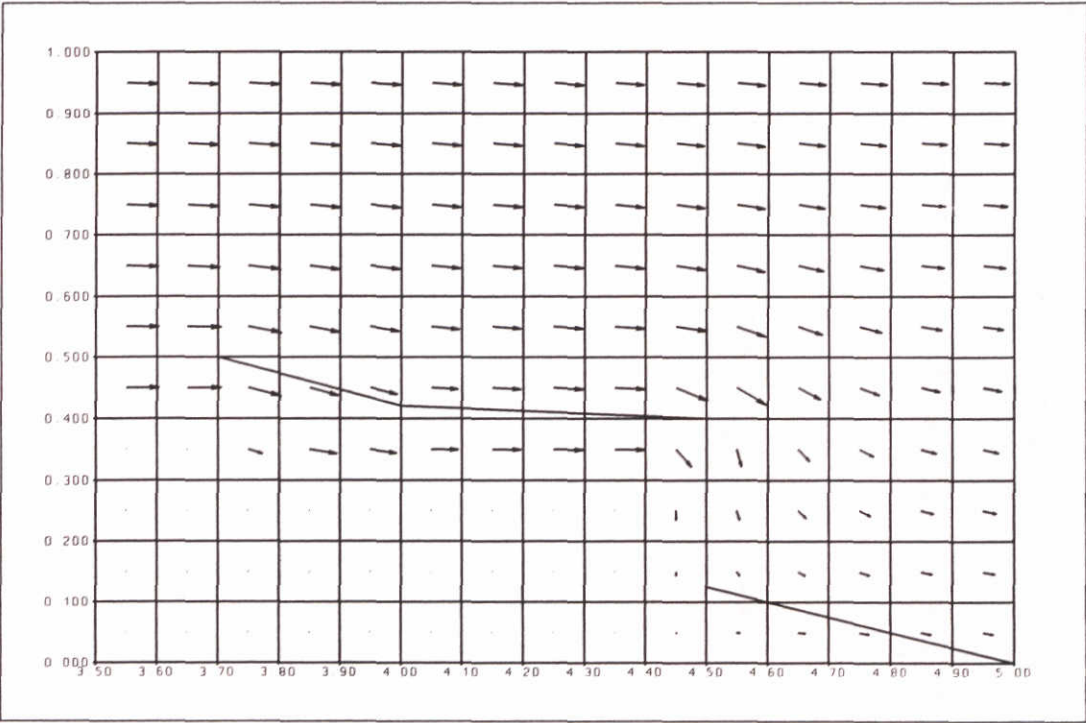


Figure 22 Right part of the structure

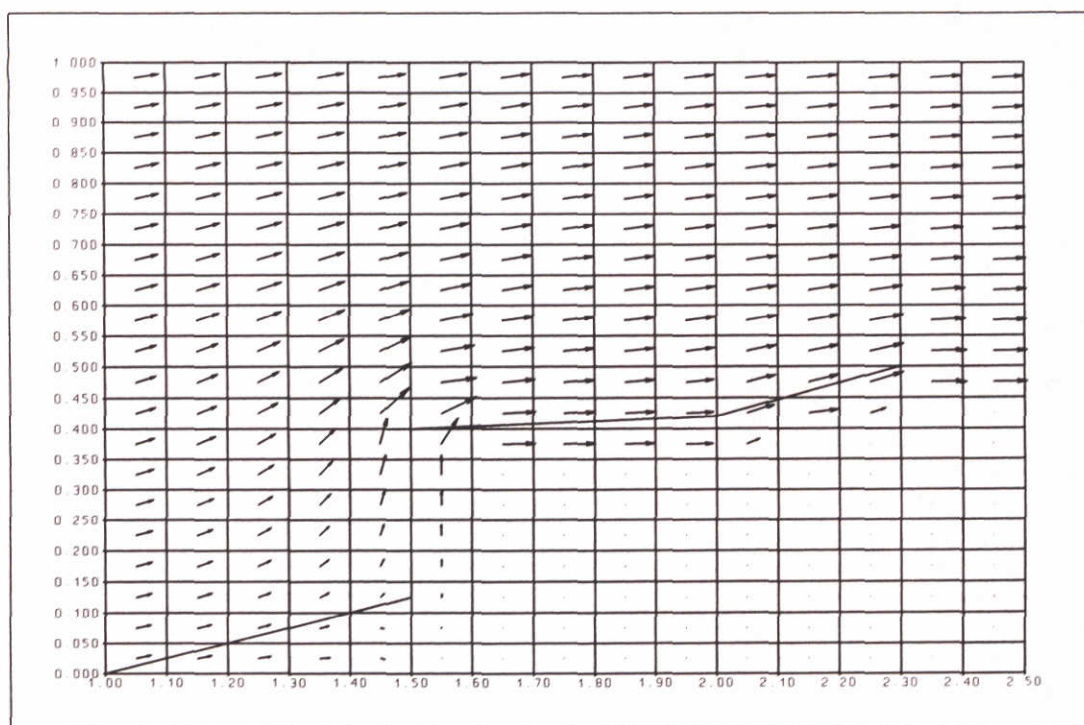


Figure 23 Reduced grid size in vertical direction

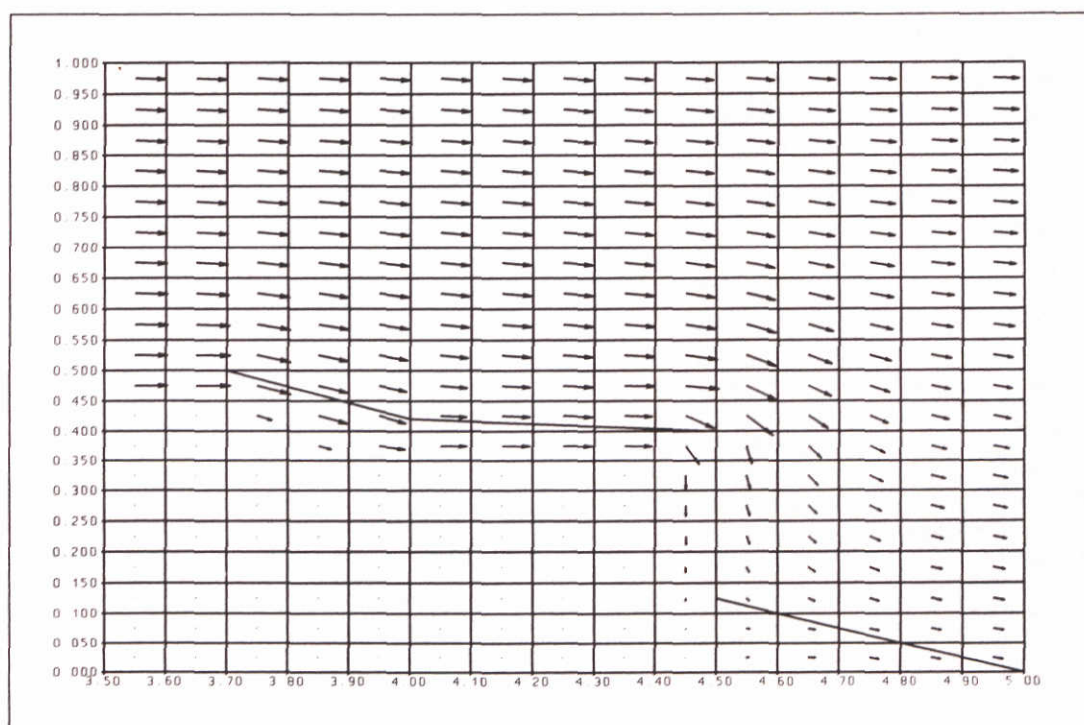


Figure 24 Reduced cell size in vertical direction

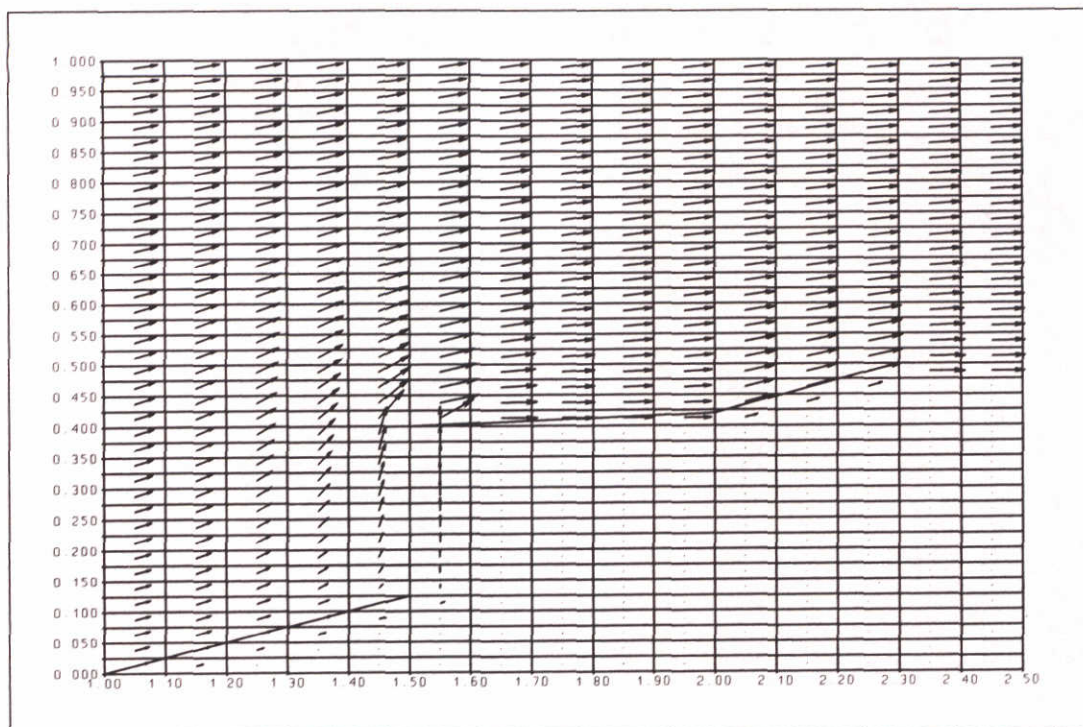


Figure 25 Cell width in y-direction reduced with factor 1/4

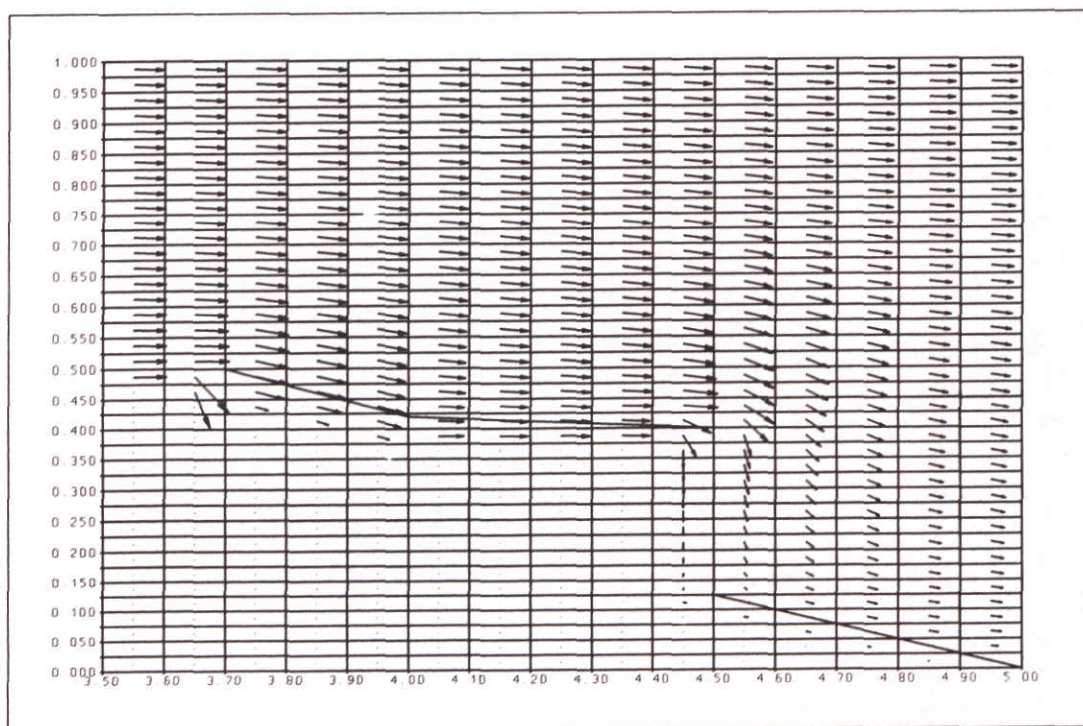


Figure 26 Cell width in y-direction reduced with factor 1/4

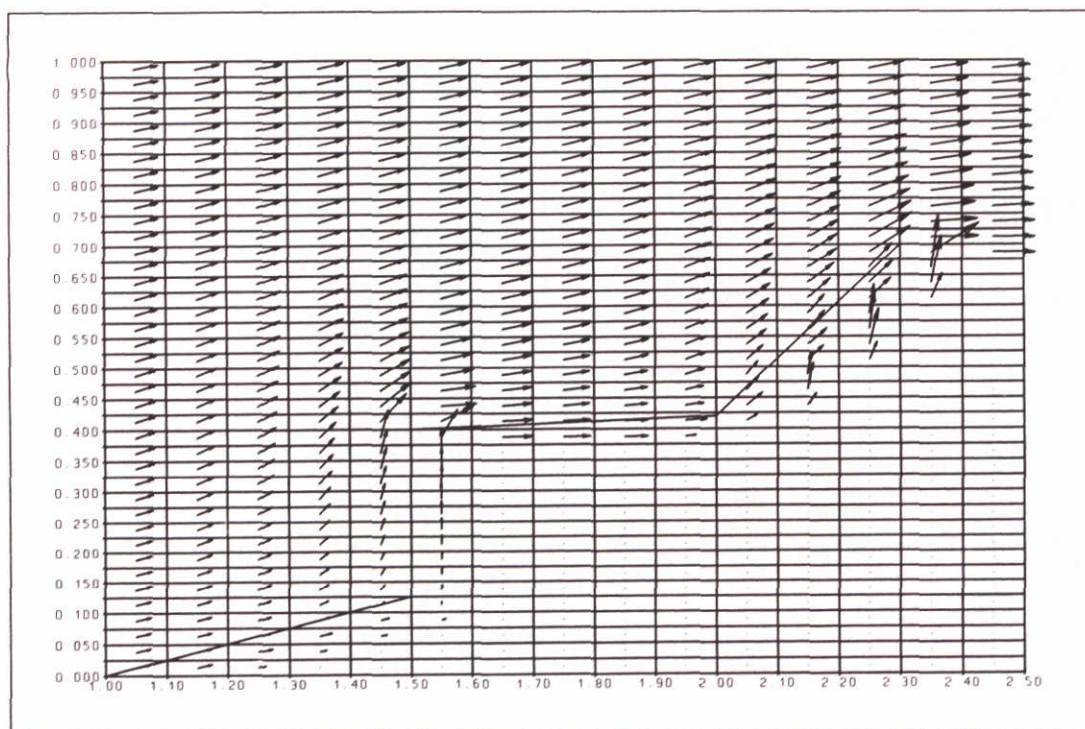


Figure 27 Cells of category 4 included

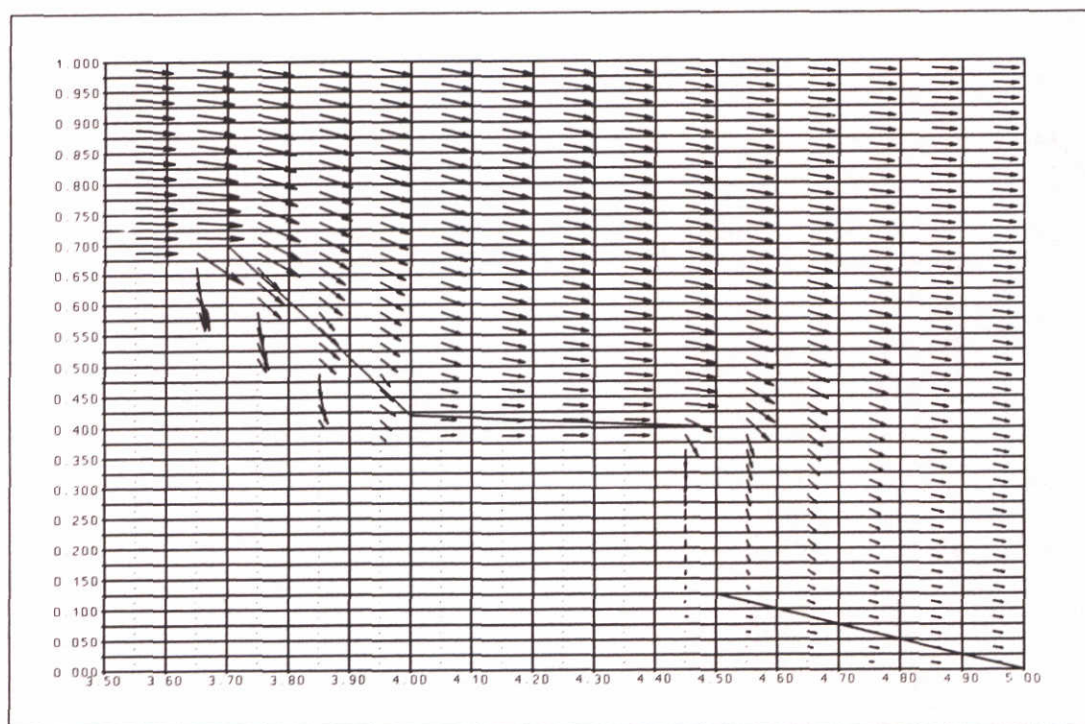


Figure 28 Cells of category 8 included

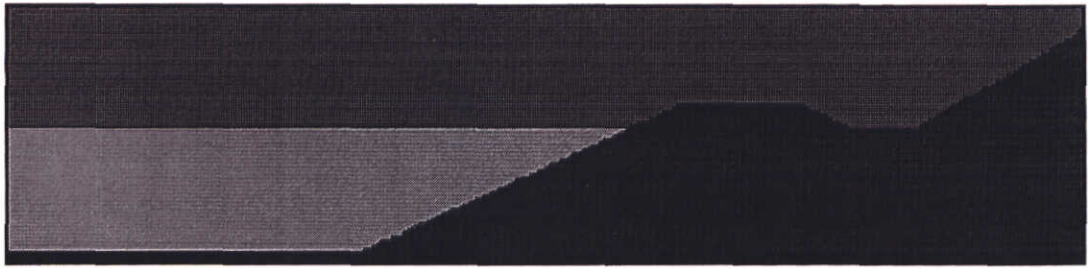


Figure 29 Initial condition

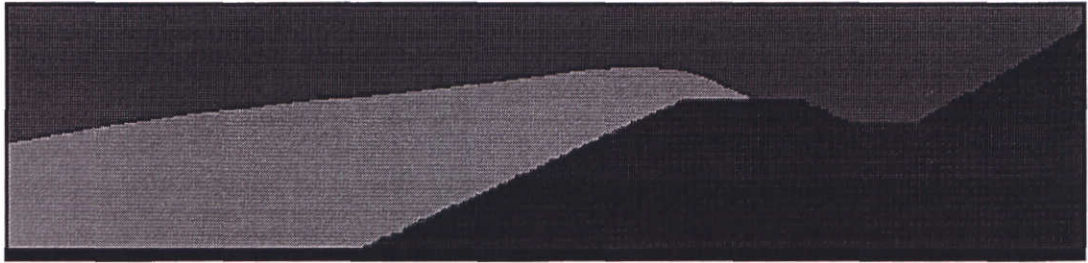


Figure 30 Overtopping wave

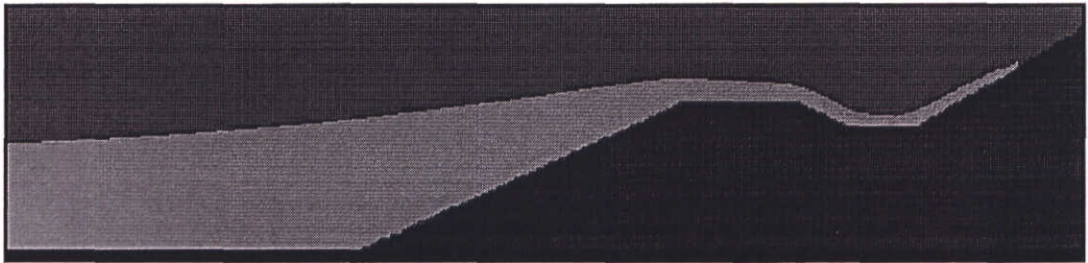


Figure 31 Overtopping and second run up

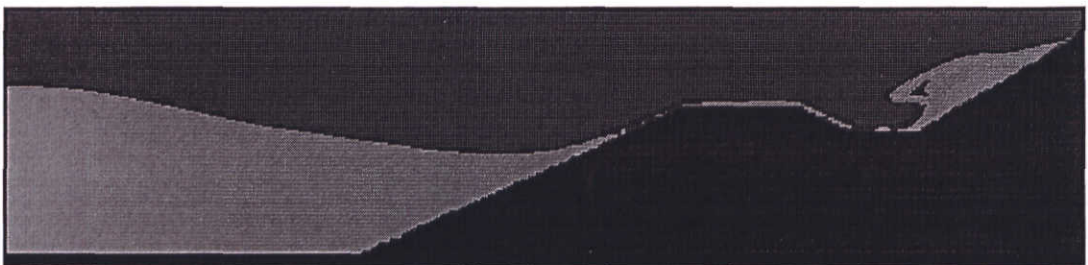


Figure 32 Backwash on second slope

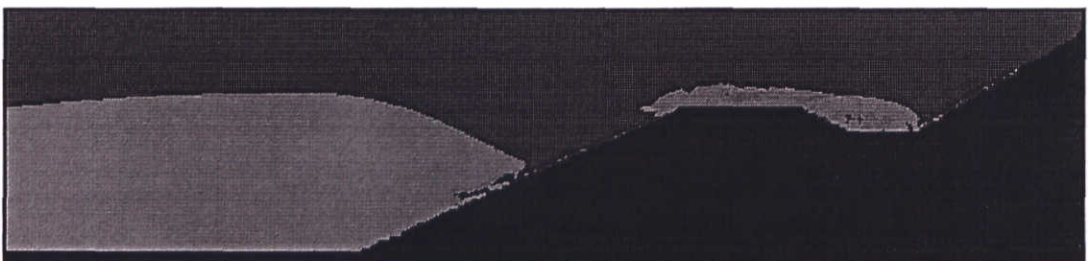


Figure 33 Canal filled up

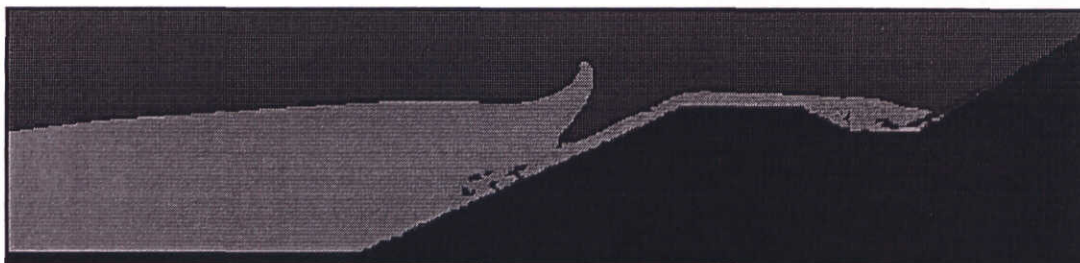


Figure 34 Second wave meets backwash

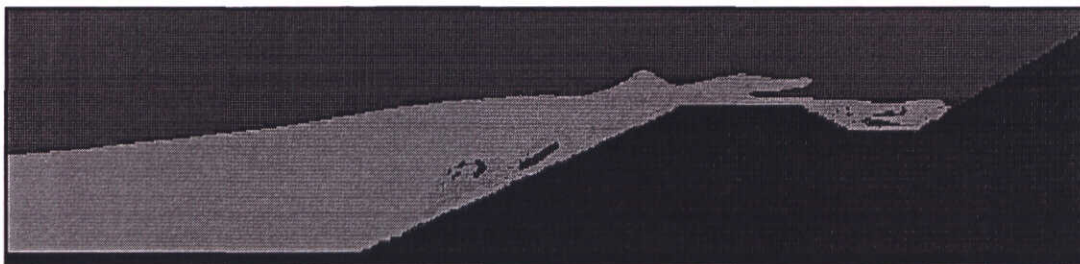


Figure 35 Velocity reversed on the top of the structure

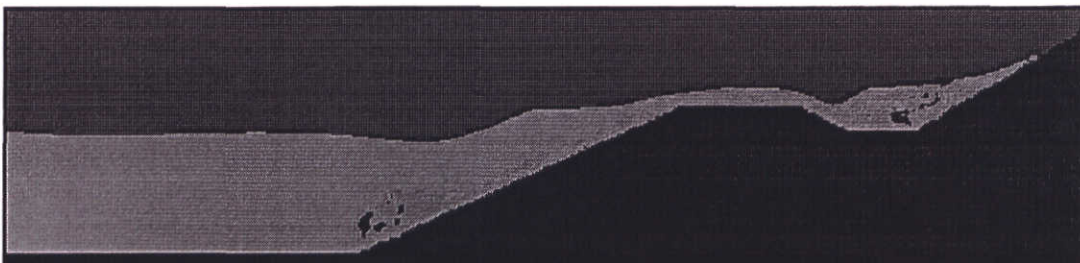


Figure 36 Start of run up on second slope

2.5 Overtopping-boundary conditions and applicability

By modelling a low crested structure, overtopping can be simulated by SKYLLA. Since the kind of flow conditions left and right of the top can be very different, the computational costs can grow dramatically. This problem can, for example, arise if at the right of the top a thin layer of water runs down the slope. In order to accurately model this thin layer, the size of the cells should be small over the entire length of the falling part of the slope. However, the grid dimensions cannot be defined locally in SKYLLA, so that a necessary reduction in cell size at the right of the top will automatically introduce smaller cells at the left. Here larger cells could for example suffice for an accurate computation. As the CPU time per simulated time step is approximately proportional to the third power of the number of wet cells in the domain, care should be taken not to define very small cells in regions in which the velocity remains relatively small.

Under certain conditions this problem can be dealt with in an economical way.

In order to simulate overtopping in SKYLLA the problem is now split into two separate problems, the seaward part and the polder part. The two models in which these problems are to be solved are numbered 1 and 2 in Figure 37.

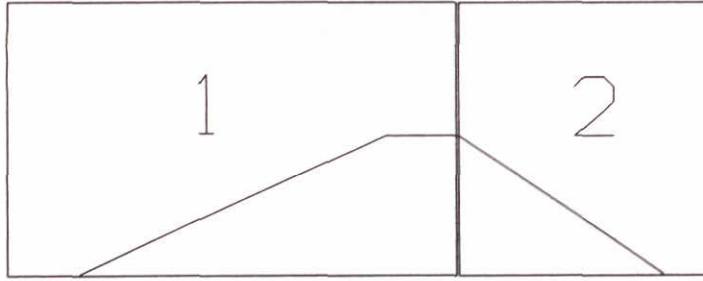


Figure 37 Two-model approach

As the Navier-Stokes equations describing incompressible flow are essentially parabolic, there is an interdependence of all quantities in a connected wet region.

By describing the flow at the top of the structure using the shallow water equations, one can show that in the case of horizontal velocities which are larger than \sqrt{gh} the fluid at the left is not influenced by fluid quantities at the right. As the overtopping layer of water is expected to be relatively thin, the vertical velocities within the layer at the top are expected to be small. Furthermore, the free-slip boundary condition and the small viscosity justify the approximation using depth-averaged shallow water approximation.

Since the shallow water equations suggest that flow quantities do not depend on downstream flow in the supercritical case we assume the dependence to be small in the case when Navier-Stokes equations are used.

The criterion $u > \sqrt{gh}$ is now used as a sufficient condition for the use of the two-model approach.

2.6 Numerical implementation

We assume that at the right boundary of model 1 the flow of the overtopping water is supercritical. In order to minimize the influence of the boundary treatment at the right we impose the following boundary conditions:

$$\frac{\partial u}{\partial x} = 0 \quad (7)$$

$$\frac{\partial v}{\partial x} = 0 \quad (8)$$

Furthermore, we will set the F function equal to 0 in the last (virtual) column. All fluid fluxed into this column will immediately vanish, effectively simulating a black hole.

In Figure 38 the two last columns are indicated. In the registration column the velocities and F values are stored during the computation. These values are to be used as input for the second model.

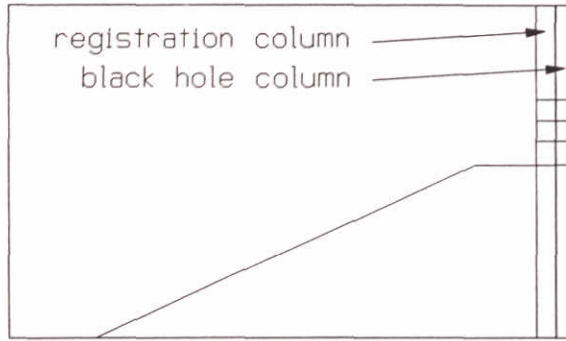


Figure 38 Virtual cells and registration cells

The continuity equation at the last wet column becomes:

$$\Delta y_j (u_{imaxj}^{q+1} - u_{imax-1j}^{q+1}) + \Delta x_{imax} (v_{imaxj}^{q+1} - v_{imaxj-1}^{q+1}) = 0 \quad (9)$$

Boundary condition (2.5.1) is discretized as:

$$u_{imaxj}^{q+1} - u_{imax-1j}^{q+1} = 0$$

reducing the continuity equation to:

$$v_{imaxj}^{q+1} - v_{imaxj-1}^{q+1} = 0 \quad (10)$$

Boundary condition (2) is discretized as:

$$v_{imax+1j}^q = v_{imaxj}^q$$

The velocities needed to determine \tilde{u}_{imaxj} are now available.

The pressure boundary condition becomes:

$$\Delta t \left(\frac{P_{imaxj+1}^{q+1} - P_{imaxj}^{q+1}}{\frac{1}{2}(\Delta y_{j+1} + \Delta y_j)} - \frac{P_{imaxj}^{q+1} - P_{imaxj-1}^{q+1}}{\frac{1}{2}(\Delta y_j + \Delta y_{j-1})} \right) = \tilde{v}_{imaxj} - \tilde{v}_{imaxj-1}$$

In Figure 39 we show the velocities and the positions of the F values (the small circles). The values found at these locations have to be stored at each time step.

Since the time steps and the grid sizes in the calculations for the right and the left part of the problem will not be the same, the data written onto the file used in the second calculation cannot directly be used as input. We use linear interpolation in time and space to determine the values of u, v and F at the overtopping inflow boundary.

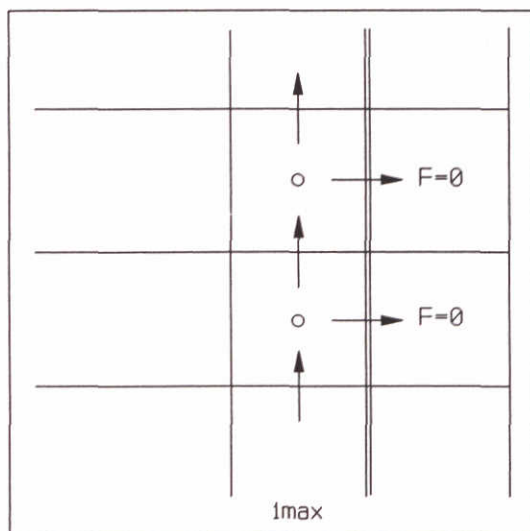


Figure 39 Black holes in virtual column

The condition that the flow has to be supercritical at the top can be relaxed by taking different positions for the registration column and the black hole column as shown in Figure 40.

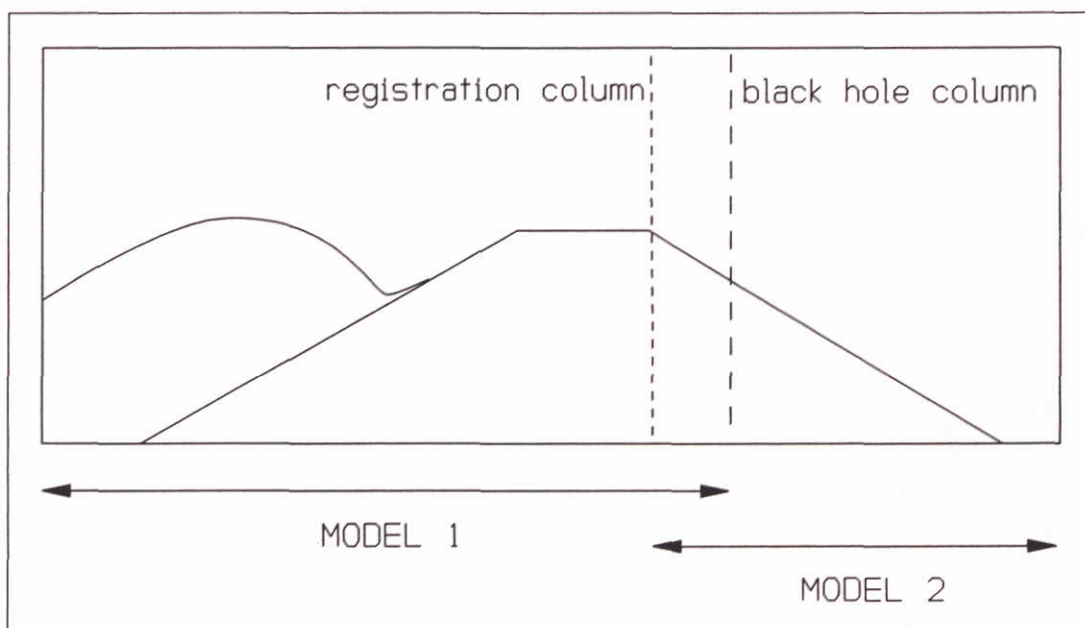


Figure 40 Registration and black hole column at different locations

We use the assumption that flow at the top of the dike is not influenced by the flow at the 'black hole' boundary.

By defining model 1 as indicated in Figure 40 we can use the model in which the velocity of the overtopping water is subcritical. With the use of this boundary condition we only need to enlarge slightly the domain for the first calculation compared to the two-model approach as shown in Figure 37. The extra CPU time needed will not be significant if relatively large cells are used at the right of the registration column.

We should realize, however, that in a strict sense the registered velocities and F-values at the boundary can not be used to prescribe them at the boundary of model 2 unless the overtopping is supercritical. The problem is caused by waves which travel in the direction opposite to the subcritical overtopping flow. On arrival at the inflow boundary these waves will fully reflect. However, in reality these waves should be transmitted through the boundary and leave model 2.

In practical situations the approach with a boundary as indicated in Figure 40 will probably suffice provided the velocity of the overtopping water will not become much smaller than the critical velocity $u_c = \sqrt{gh}$ where h is the thickness of the overtopping layer.

2.7 Tests with overtopping-boundary conditions

In this section we will show the results of two tests that were used to verify the overtopping boundary condition.

In the first of these tests we used the inflow boundary condition with a hand made file where the influx was prescribed as a constant over a small section of the left boundary. The other boundaries of the computational domain were closed. In Figure 41 the snapshots taken from the animation show the incoming jet of water until it hits the shallow layer of water on the bottom of the tank. The parabolic shape of the jet matches exactly the prescribed horizontal inflow velocity.

In the second test overtopping is simulated with the two-model approach. In Figure 42 we see the structure the way it is modelled for the "left" SKYLLA computation. The column in which the velocities and the F values are registered, is located left of the edge where the slope begins to fall. The first overtopping wave was just at that position when the snapshot was taken. At the right boundary of the left model we use a black hole outflow boundary. As can be seen in Figure 42 there is initially fluid at rest right from the structure. As long as the fluid is at rest, it is not influenced by the black hole condition as all this condition does is prescribe the outflow velocity to be independent of x near the boundary.

Figure 43 shows the overtopping wave some time later. Here we see that the water on the right, which was initially at rest, is now vanishing through the black hole boundary. The jet of water generated by the overtopping wave is also vanishing into the black hole boundary.

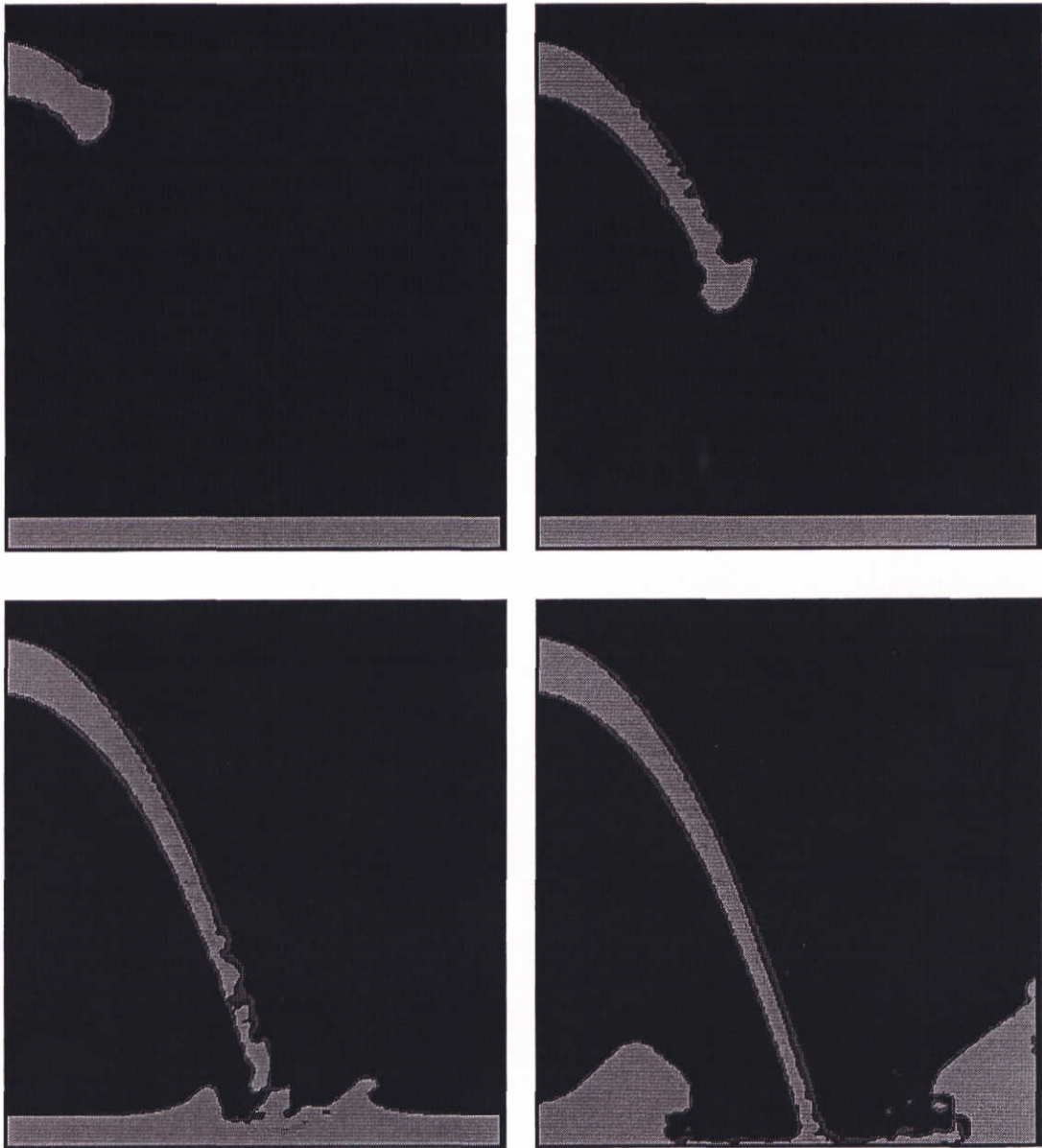


Figure 41 Test for overtopping inflow boundary

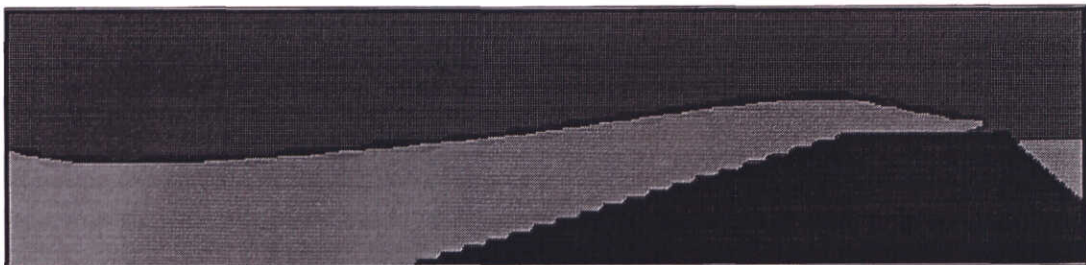


Figure 42 First overtopping wave

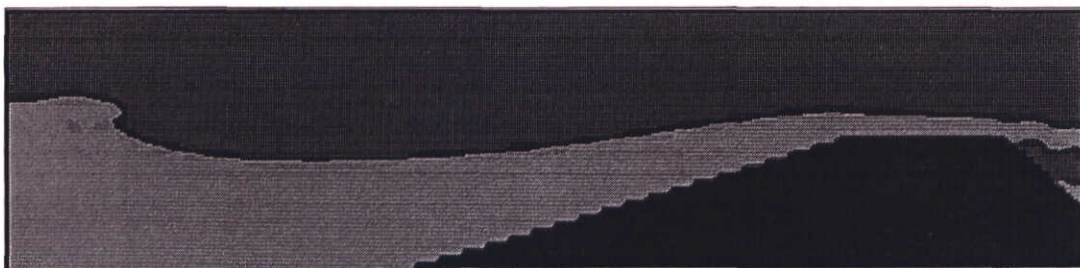


Figure 43 Jet vanishes into black hole column



Figure 44 First water entering the right model

The right part of the model is shown in Figure 44. The left boundary is located at the position of the registration column in the computation for the left part of the model. The velocities and F values, which were registered there, are now used to prescribe these quantities at the inflow boundary.

At the right we also use a black hole boundary condition to get rid of the water which has entered the model. In Figure 44 we also see that the falling slope modelled here is somewhat steeper than the slope used in the computation for the left part of the model. Note that all which is on the downstream side of the registration column, is only used to make the water leave the model. It should not affect what is registered if the assumption holds that the flow on the top of the structure is supercritical.

In Figure 45 we see that the water which was initially at rest on the right of the left model has vanished. Furthermore, we see from the shape of the parabola that the velocity of the overtopping water has decreased. The situation in the right model at approximately the same time is shown in Figure 46. Here we see that the jet generated by the overtopping water looks quite different from the result in the left model. The differences are caused by the fact that the grid used in the right model is much smaller than the grid used in the left model. The fact that the jet has split into a part which is falling freely and a part which is running down the slope, is explained in the next section.

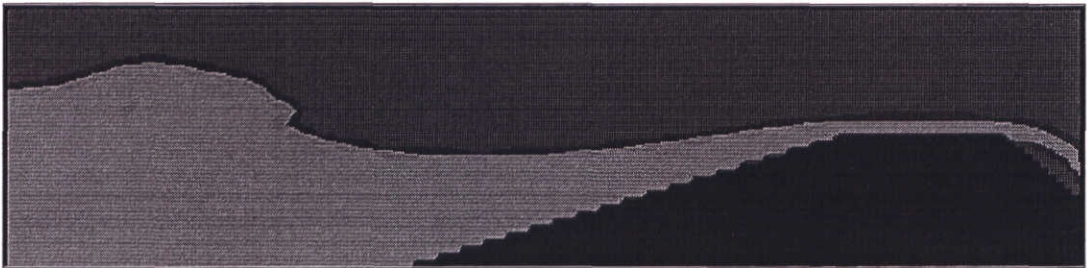


Figure 45 Decreasing velocity at the top



Figure 46 Jet has split

In Figure 47 the velocity of the overtopping water has decreased even more and the layer of water now remains stuck to the slope. The same can now be seen for the right part of the computation in Figure 48. Here a second jet of water is released from the slope before it vanishes into the black hole column.

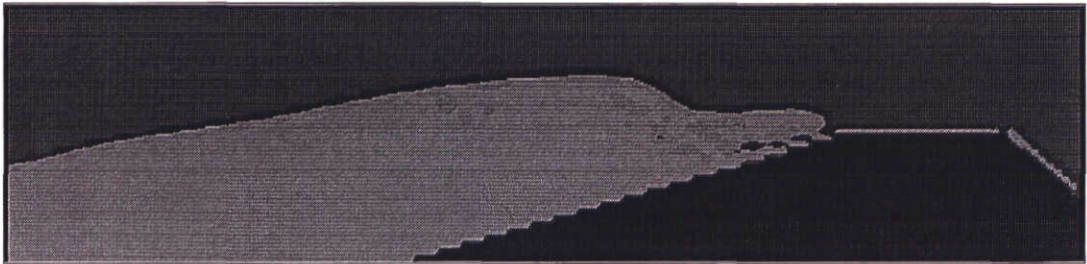


Figure 47 Reduced velocity of overtopping layer of water

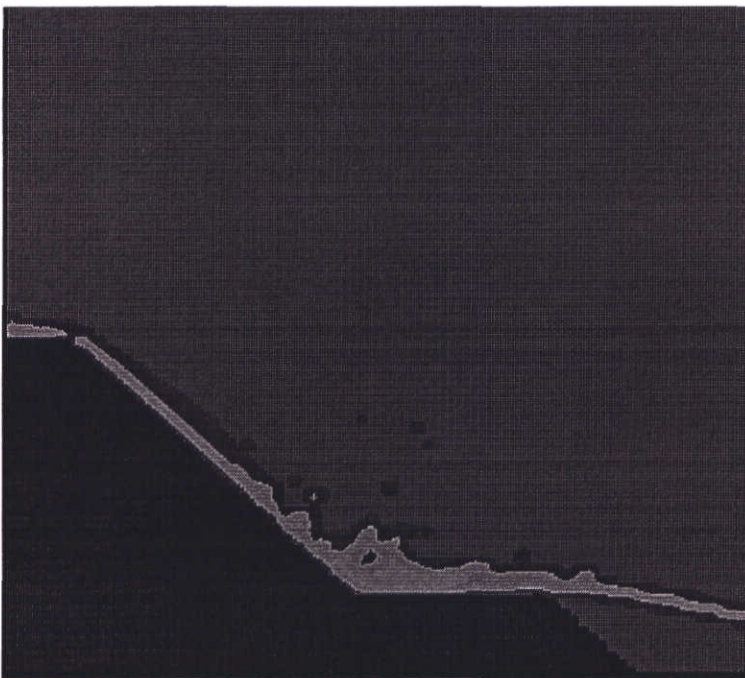


Figure 48 Second jet on falling slope

In Figure 49 we see the second overtopping wave, a part of which is released from the slope at the edge. A snapshot of the resulting flow in the right model is given in Figure 50. The last two figures 51 and 52 show the situation some moments later.

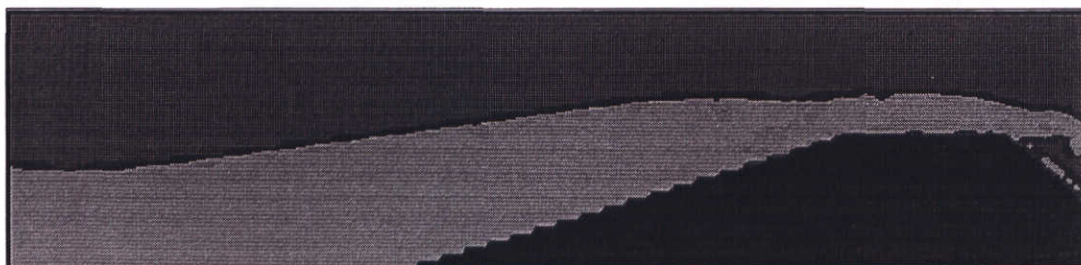


Figure 49 Second overtopping wave

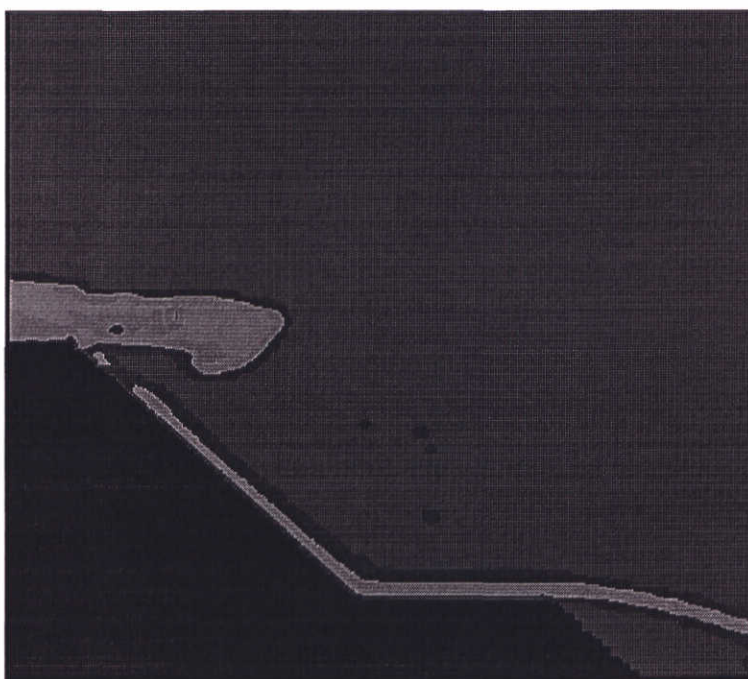


Figure 50 Second overtopping wave in right model

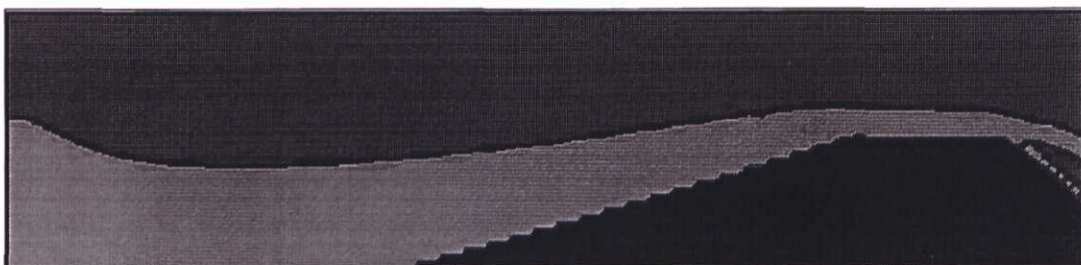


Figure 51 Jet of water after overtopping

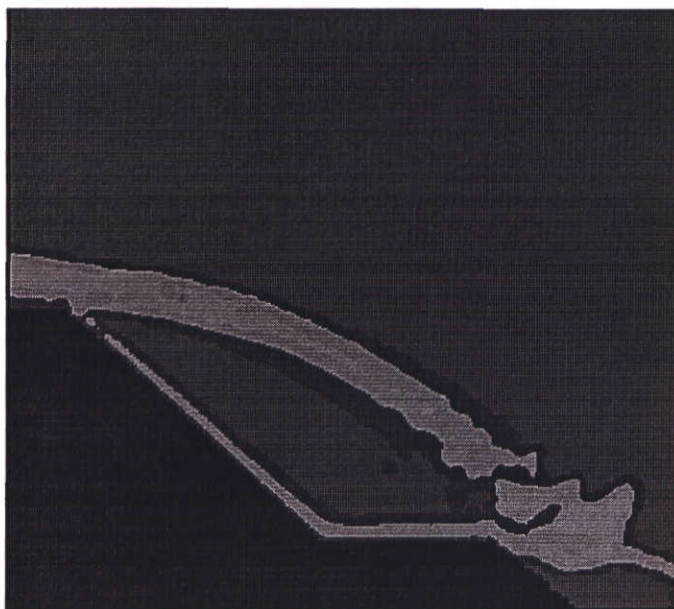


Figure 52 Split jets at edge in right model

Figure 53 which is a snapshot of the situation in the right model some moments later, shows that the black hole boundary can cause disturbances. Although they seem serious the disturbance leaves the domain rather quickly. However it is advisable to take some distance between the black hole boundary and the registration column.

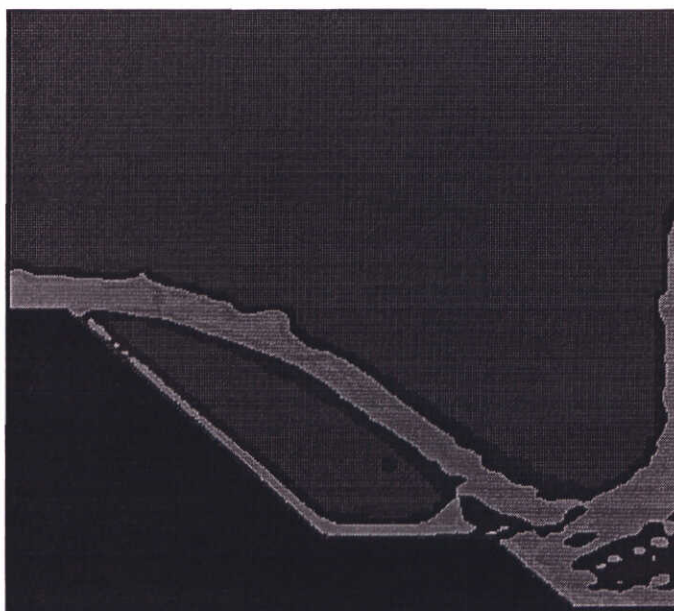


Figure 53 Disturbance at boundary

2.8 Unresolved problems at sharp edges

If water flows in a region bounded by a slope as indicated in Figure 54, the contradicting boundary conditions at the edge where the direction of the slope is discontinuous can pose problems.

Let us first consider the case in which the entire domain above the slope is filled with water and assume free-slip boundary conditions at the slope. Left of the edge the impermeability condition states that the velocity at the slope has no component in normal direction:

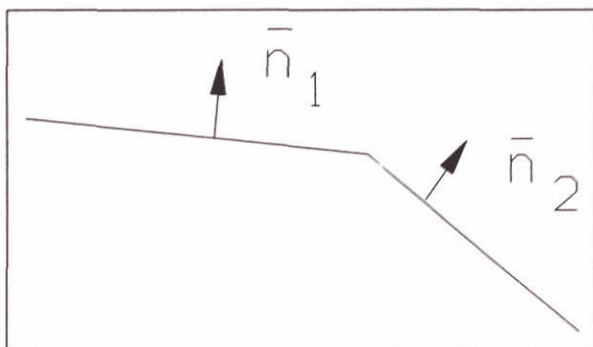


Figure 54 Angle in a slope

$$\mathbf{u} \cdot \mathbf{n}_1 = 0$$

At the right part of the slope the condition becomes:

$$\mathbf{u} \cdot \mathbf{n}_2 = 0$$

If we assume the velocity to be a continuous function of the arc length of the curve which represents the slope, this immediately leads to:

$$\mathbf{u} = \mathbf{0} \text{ at the edge.}$$

In the case when there is no water on the right of the edge, a jet of water coming from the left should separate from the slope after reaching the edge. In that case the water is not influenced by the boundary conditions on the right of the edge.

In SKYLLA this is not realized as is illustrated in Figure 55. Here we see the virtual velocities indicated by double arrows with a different line style for the cells on the left and right of the edge. At the moment that the cell on the right of the edge receives water from the left or the top neighbouring cell, the virtual velocities which prescribe the impermeability and the free-slip boundary condition will be set. In discretizing the momentum equation for the velocity components at the top and the right boundary of this cell these conditions will be prescribed and the fluid will remain in contact with the slope.

If the layer of water streaming down the slope is thick measured in cell heights, it may well be the case that a part of the jet will separate from the slope; another part however, will remain on the slope.

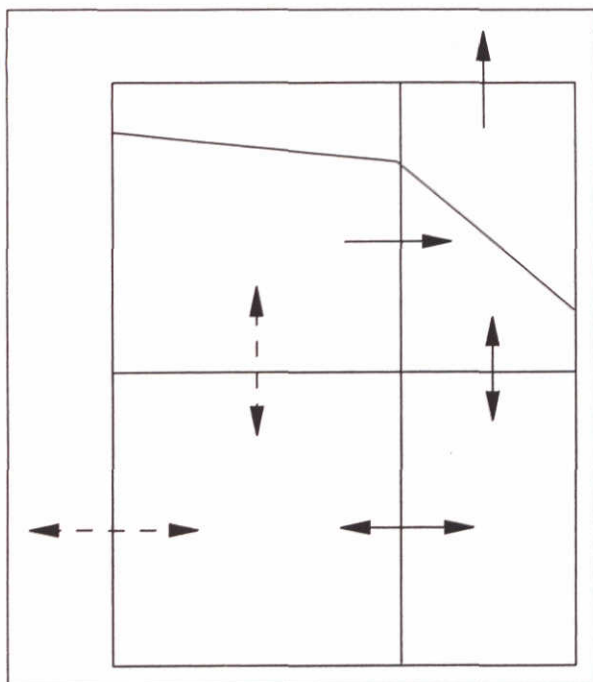


Figure 55 Virtual velocities at edge

In Appendix B some suggestions are given on how the problems at the sharp edges could be dealt with.

3 Conclusions and recommendations

The results of the work presented here show how the free-slip and the impermeability boundary conditions were implemented in SKYLLA. They also show that these conditions are indeed satisfied at the boundaries.

The SKYLLA code we started with enabled the modelling of climbing slopes using cell categories 1 to 4. By implementing ten new categories the kinds of slopes that can now be modelled in SKYLLA has increased significantly. In addition, the program has been made more user-friendly by allowing the user to model a slope by giving a polygon which prescribes the impermeable surface of the structure.

In order to reduce the computational effort needed to simulate overtopping waves the option to split the domain in two has been introduced in SKYLLA. This allows the user to define a fine grid in one part of the model without influencing the grid in the other part. The boundary conditions introduced for this purpose can also be used without the coupling with another computation. The tests show that the overtopping boundary condition works properly.

However, the tests have also revealed shortcomings of the boundary conditions now implemented. At an edge on a slope the boundary conditions tend to attract the water to the boundary of the slope refusing a jet of water to be released from the slope at the edge. This is a direct result of prescribing the normal velocity of the water at the slope to be zero.

If the program is to be used for the modelling of overtopping waves this problem should be addressed first.

The same shortcomings will also hinder the modelling of a recirculation zone behind a submerged structure which can become important for future applications.

References

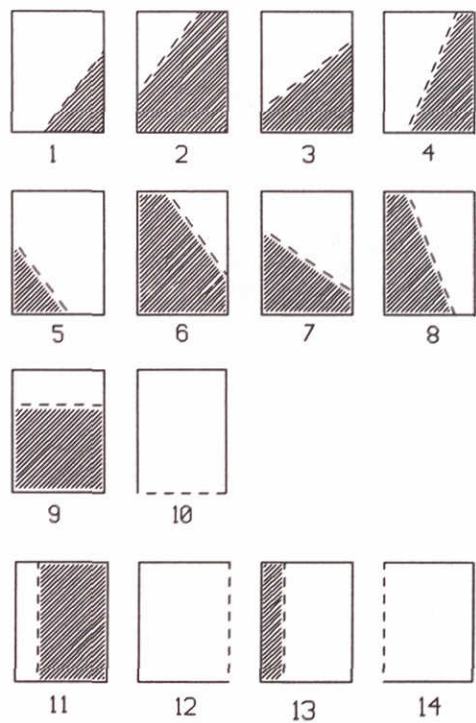
- Ashgriz, N. and J.Y. Poo (1991). FLAIR: Flux Line-Segment Model for Advection and Interface Reconstruction. *J. of Comp. Physics* 93, pp.449-468.
- Broekens, R.D. and H.A.H. Petit (1991). SKYLLA: Wave Motion in and on Coastal Structures. Feasibility study on the applications of SAVOF, MAST-G6S report, DELFT HYDRAULICS.
- Gent, M.R.A. van (1991). Formulae to describe porous flow. *Communications on Hydraulic and Geotechnical Engineering*, ISSN 0169-6548, No. 92-2, Delft University of Technology.
- Klein Breteler, M. and H.A.H. Petit (1993). SKYLLA: Proposal for further developments and validation (in Dutch: Plan voor verdere ontwikkeling en validatie). Report H 1780, DELFT HYDRAULICS.
- Meer, J.W. van der, H.A.H. Petit, P. van den Bosch, G. Klopman and R.D. Broekens (1992). Numerical simulation of wave motion on and in coastal structures. *Proc. ICCE'92, Venice, Italy*.
- Nichols, B.D. and C.W. Hirt (1980). SOLA-VOF: A Solution Algorithm for Transient Fluid Flow with Free Boundaries. Report LA-8355, Los Alamos Scientific Laboratory.
- Petit, H.A.H. and P. van den Bosch (1992). SKYLLA: Wave Motion in and on Coastal Structures; Numerical analysis of program modifications. MAST-G6S report, DELFT HYDRAULICS.
- Petit, H.A.H., P. van den Bosch and M.R.A. van Gent (1993). SKYLLA: Wave Motion in and on Coastal Structures; Implementation and verification of modified boundaries. Report H1780, DELFT HYDRAULICS.
- Rienecker, M.M. and J.D. Fenton (1981). A Fourier approximation method for steady water waves. *Journal of Fluid Mechanics*. Vol. 104, pp. 119-137.
- Gent, M.R.A. van, H.A.H. Petit and P. van den Bosch (1993). SKYLLA: Wave Motion in and on Coastal Structures; Implementation and verification of flow on and in permeable structures. Draft report H1780, DELFT HYDRAULICS.
- Gent, M.R.A. van, J.P. de Waal, H.A.H. Petit and P. van den Bosch (1994). SKYLLA: Wave Motion in and on Coastal Structures; Verification of kinematics of waves breaking on an offshore bar. Report H1780 DELFT HYDRAULICS.
- Hindmarsh, A.C., P.M. Gresho and D.F. Griffiths (1984). The Stability of Explicit Time-Integration for certain Finite Difference Approximations of the Multi-Dimensional Advection-Diffusion Equation. *Int. J. for Numerical Methods in Fluids*, Vol.4, pp. 853-897.

Appendix A

Numerical treatment of climbing and falling slopes in SKYLLA

Numerical treatment of climbing and falling slopes in SKYLLA

In order to be able to model a more general structure in SKYLLA the program has to be extended with the option of falling slopes. The types of cells that should enable us to do that are indicated in Figure A1.



Some special cases where the slope intersects the cell at a corner point can be categorized in the categories as shown in Figure A1, with respect to the equations that state the impermeability of the slope and the free slip property. These cells are shown in Figure A2 for the case of a climbing slope. In the case of a falling slope these special cases are indicated in Figure A3.

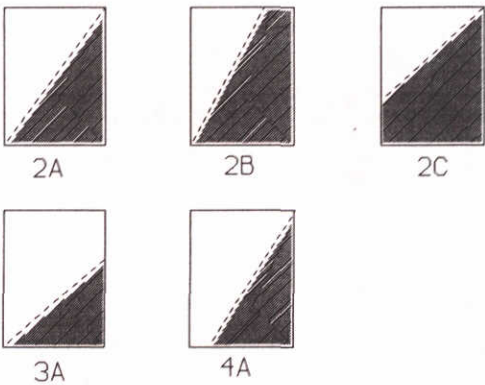


Figure A1 General cell categories

Figure A2 Special cases / climbing slope

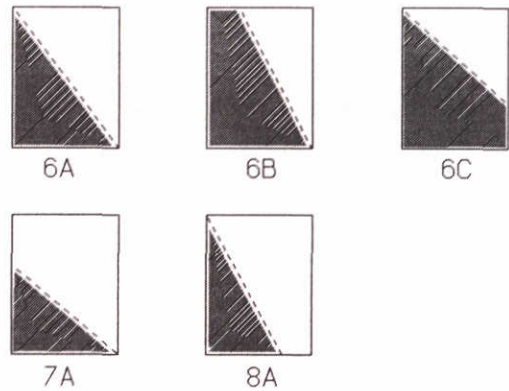


Figure A3 Special cases / falling slope

NEIGHBOURS ANTI-CLOCKWISE		NEIGHBOURS CLOCKWISE
2,2B,4,11	1	2,2C,3,9
1,3,3A,9	2	1,4,4A,11
2A,2C,4A,10,12	2A	2A,2B,3A,10,12
2A,2C,4A,10,12	2B	1,4,4A,11
1,3,3A,9	2C	2A,2B,3A,10,12
1,3,3A,9	3	2,2C,3,9
2A,2C,4A,10,12	3A	2,2C,3,9
2,2B,4,11	4	1,4,4A,11
2,2B,4,11	4A	2A,2B,3A,10,12
6,6C,7,9	5	6,6B,8,13
5,8,8A,13	6	5,7,7A,9
6A,6B,7A,10,14	6A	6A,6C,8A,10,14
5,8,8A,13	6B	6A,6C,8A,10,14
6A,6B,7A,10,14	6C	5,7,7A,9
6,6C,7,9	7	5,7,7A,9
6,6C,7,9	7A	6A,6C,8A,10,14
5,8,8A,13	8	6,6B,8,13
6A,6B,7A,10,14	8A	6,6B,8,13
1,3,3A,6,6C,7,9	9	2,2C,3,5,7,7A,9
2A,2C,4A,6A,6B,7A,10	10	2A,2B,3A,6A,6C,8A,10
2,2B,4,11	11	1,4,4A,11
2A,2C,4A,12	12	2A,2B,3A,12
5,8,8A,13	13	6,6B,8,13
6A,6B,7A,14,	14	6A,6C,8A,14

In the table above we can see which cells can be coupled by traversing in clockwise or anti-clockwise direction along the surface of the structure with respect to a point inside the structure. Here it can be seen that we made the choice that in going from a climbing part of the surface to a falling part, or the other way around, we always encounter a horizontal part.

We will now give the equations from which the virtual velocities can be determined. The pressure boundary conditions for these cells will be given as well.

In order to be able to model the combination of an impermeable slope and a rubble structure we introduce n_{ij} which is the porosity of cell (ij). We define

$$n_{i+\frac{1}{2},j} = \frac{\Delta x_i n_{i+1,j} + \Delta x_{i+1} n_{ij}}{\Delta x_i + \Delta x_{i+1}}, \quad n_{ij+\frac{1}{2}} = \frac{\Delta y_j n_{ij+1} + \Delta y_{j+1} n_{ij}}{\Delta y_j + \Delta y_{j+1}},$$

$$\gamma_{ij} = \frac{n_{i+\frac{1}{2},j}}{1 + C_M(n_{i+\frac{1}{2},j})} \quad \text{and} \quad \lambda_{ij} = \frac{n_{ij+\frac{1}{2}}}{1 + C_M(n_{ij+\frac{1}{2}})}.$$

Category I: No virtual velocities.

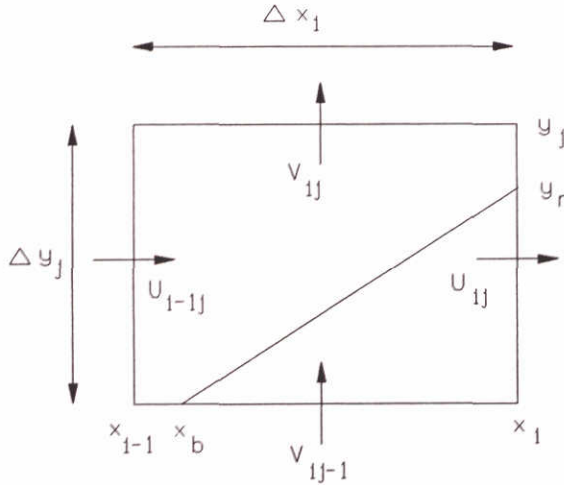


Figure A4

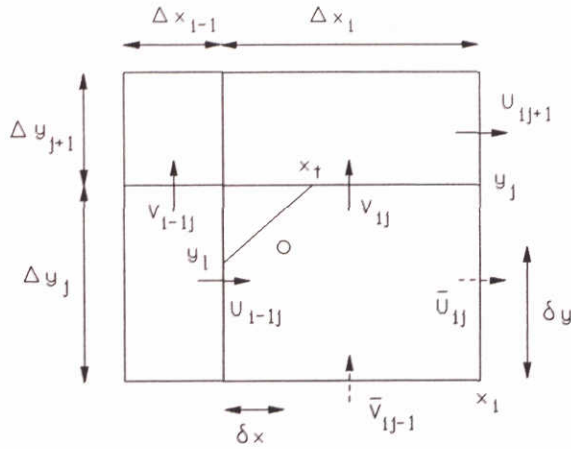
For this cell the continuity equation becomes:

$$(y_j - y_r)u_{ij}^{n+1} - \Delta y_j u_{i-1,j}^{n+1} + \Delta x_i v_{ij}^{n+1} - (x_b - x_{i-1})v_{ij-1}^{n+1} = 0$$

From this equation we can derive the pressure boundary condition:

$$\begin{aligned} & \frac{2\Delta t(y_j - y_r)}{\Delta x_{i+1} + \Delta x_i} \gamma_{ij} (P_{i+1,j}^{n+1} - P_{ij}^{n+1}) - \frac{2\Delta t\Delta y_j}{\Delta x_i + \Delta x_{i-1}} \gamma_{i-1,j} (P_{ij}^{n+1} - P_{i-1,j}^{n+1}) + \\ & \frac{2\Delta t\Delta x_i}{\Delta y_{j+1} + \Delta y_j} \lambda_{ij} (P_{ij+1}^{n+1} - P_{ij}^{n+1}) - \frac{2\Delta t(x_b - x_{i-1})}{\Delta y_j + \Delta y_{j-1}} \lambda_{ij-1} (P_{ij}^{n+1} - P_{ij-1}^{n+1}) = \\ & (y_j - y_r)\tilde{u}_{ij} - \Delta y_j \tilde{u}_{i-1,j} + \Delta x_i \tilde{v}_{ij} - (x_b - x_{i-1})\tilde{v}_{ij-1} \end{aligned} \quad (A-1)$$

Category 2:



Let $\mathbf{n}=(n_1,n_2)^T$ be the unit normal vector at the slope and $\boldsymbol{\tau}=(\tau_1,\tau_2)^T$ be the unit tangential vector. Linear extrapolation of u and v velocity components is used and yields a first order accurate expression for the free-slip equation $\frac{\partial u_t}{\partial n}=0$ at the collocation point which is indicated at the slope in Figure A6. Here $u_t=(\mathbf{u} \cdot \boldsymbol{\tau})$.

Figure A5

$$n_1 \tau_1 \left(\frac{\bar{u}_{ij} - u_{i-1j}}{\Delta x_i} - \frac{v_{ij} - \bar{v}_{ij-1}}{\Delta y_j} \right) + 2n_1 \tau_2 \frac{v_{ij} - v_{i-1j}}{\Delta x_i + \Delta x_{i-1}} + 2\tau_1 n_2 \frac{u_{ij+1} - \bar{u}_{ij}}{\Delta y_{j+1} + \Delta y_j} = 0 \quad (\text{A-2})$$

By using linear extrapolation a second order expression is found for the normal component of the velocity at the collocation point on the slope, which must equal zero:

$$\begin{aligned} n_1 \left[u_{i-1j} + \frac{\bar{u}_{ij} - u_{i-1j}}{\Delta x_i} \delta x + 2\left(\delta y - \frac{1}{2}\Delta y_j\right) \frac{u_{i-1j+1} - u_{i-1j}}{\Delta y_j + \Delta y_{j+1}} \right] + \\ + n_2 \left[v_{ij} + 2\left(\delta x - \frac{1}{2}\Delta x_i\right) \frac{v_{ij} - v_{i-1j}}{\Delta x_i + \Delta x_{i-1}} + (\delta y - \Delta y_j) \frac{v_{ij} - \bar{v}_{ij-1}}{\Delta y_j} \right] = 0 \end{aligned} \quad (\text{A-3})$$

In the program the collocation point is chosen in the centre of cell (i,j) so $\delta x = \frac{1}{2}\Delta x_i$ and $\delta y = \frac{1}{2}\Delta y_j$

In this cell conservation of mass is expressed by:

$$(x_i - x_{i-1})v_{ij}^{n+1} - (y_j - y_l)u_{i-1j}^{n+1} = 0$$

The pressure boundary equation now becomes for this cell:

$$\begin{aligned} \frac{2\Delta t(x_i - x_{i-1})}{\Delta y_{j+1} + \Delta y_j} \lambda_{ij} (P_{ij+1}^{n+1} - P_{ij}^{n+1}) - \frac{2\Delta t(y_j - y_l)}{\Delta x_i + \Delta x_{i-1}} \gamma_{i-1j} (P_{ij}^{n+1} - P_{i-1j}^{n+1}) = \\ (x_i - x_{i-1})\bar{v}_{ij} - (y_j - y_l)\bar{u}_{i-1j} \end{aligned} \quad (\text{A-4})$$

Category 3:

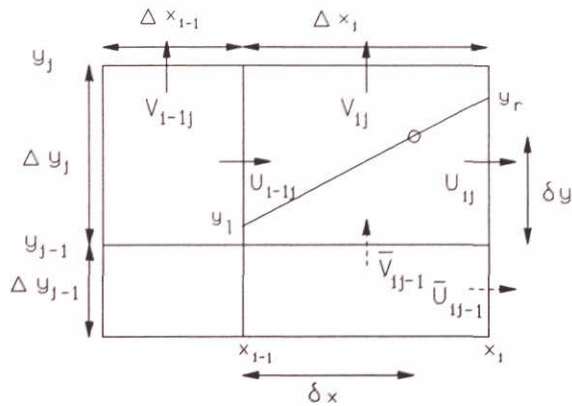


Figure A6

$$n_1 \tau_1 \left(\frac{u_{ij} - u_{i-1j}}{\Delta x_i} - \frac{v_{ij} - v_{i-1j}}{\Delta y_j} \right) + 2n_1 \tau_2 \frac{v_{ij} - v_{i-1j}}{\Delta x_i + \Delta x_{i-1}} + 2n_2 \tau_1 \frac{u_{ij} - u_{i-1j}}{\Delta y_j + \Delta y_{j-1}} = 0 \quad (\text{A-5})$$

$$n_1 \left[u_{ij} + (\delta x - \Delta x_i) \frac{u_{ij} - u_{i-1j}}{\Delta x_i} + 2(\delta y - \frac{1}{2} \Delta y_j) \frac{u_{ij} - u_{i-1j}}{\Delta y_j + \Delta y_{j-1}} \right] +$$

$$+ n_2 \left[v_{ij} + 2(\delta x - \frac{1}{2} \Delta x_i) \frac{v_{ij} - v_{i-1j}}{\Delta x_i + \Delta x_{i-1}} + (\delta y - \Delta y_j) \frac{v_{ij} - v_{i-1j}}{\Delta y_j} \right] = 0 \quad (\text{A-6})$$

The continuity equation for this cell is:

$$(y_j - y_r) u_{ij}^{n+1} + \Delta x_i v_{ij}^{n+1} - (y_j - y_r) u_{i-1j}^{n+1} = 0$$

The pressure boundary condition derived from this is:

$$\frac{2\Delta t(y_j - y_r)}{\Delta x_{i+1} + \Delta x_i} \gamma_{ij} (P_{i+1}^{n+1} - P_{ij}^{n+1}) + \frac{2\Delta t \Delta x_i}{\Delta y_{j+1} + \Delta y_j} \lambda_{ij} (P_{ij+1}^{n+1} - P_{ij}^{n+1}) +$$

$$- \frac{2\Delta t(y_j - y_r)}{\Delta x_i + \Delta x_{i-1}} \gamma_{i-1j} (P_{ij}^{n+1} - P_{i-1j}^{n+1}) = (y_j - y_r) \tilde{u}_{ij} + \Delta x_i \tilde{v}_{ij} - (y_j - y_r) \tilde{u}_{i-1j} \quad (\text{A-7})$$

Category 4:

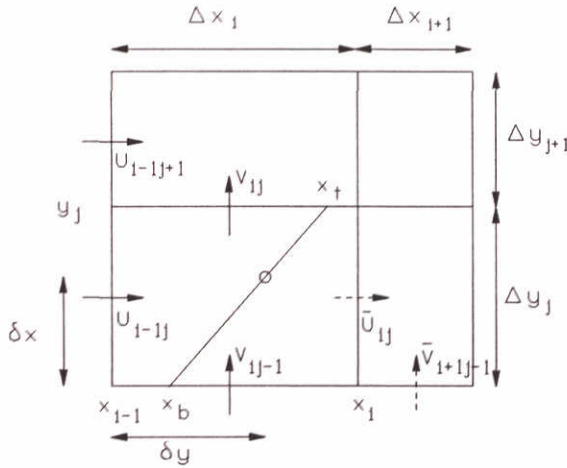


Figure A7

$$n_1 \tau_1 \left(\frac{\bar{u}_{ij} - u_{i-1j}}{\Delta x_i} - \frac{v_{ij} - v_{ij-1}}{\Delta y_j} \right) + 2n_1 \tau_2 \frac{\bar{v}_{i+1j-1} - v_{ij-1}}{\Delta x_{i+1} + \Delta x_i} + 2n_2 \tau_1 \frac{u_{i-1j+1} - u_{i-1j}}{\Delta y_{j+1} + \Delta y_j} = 0 \quad (\text{A-8})$$

$$n_1 \left[u_{i-1j} + \delta x \frac{\bar{u}_{ij} - u_{i-1j}}{\Delta x_i} + 2 \left(\delta y - \frac{1}{2} \Delta y_j \right) \frac{u_{i-1j+1} - u_{i-1j}}{\Delta y_{j+1} + \Delta y_j} \right] +$$

$$n_2 \left[v_{ij-1} + 2 \left(\delta x - \frac{1}{2} \Delta x_i \right) \frac{\bar{v}_{i+1j-1} - v_{ij-1}}{\Delta x_{i+1} + \Delta x_i} + \delta y \frac{v_{ij} - v_{ij-1}}{\Delta y_j} \right] = 0 \quad (\text{A-9})$$

The continuity equation for this cell is:

$$(x_i - x_{i-1})v_{ij}^{n+1} - \Delta y_j u_{i-1j}^{n+1} + (x_b - x_{i-1})v_{ij-1}^{n+1} = 0$$

from which the pressure condition at the boundary can be derived:

$$\begin{aligned} & \frac{2\Delta t(x_i - x_{i-1})}{\Delta y_{j+1} + \Delta y_j} \lambda_{ij} (P_{ij+1}^{n+1} - P_{ij}^{n+1}) - \frac{2\Delta t \Delta y_j}{\Delta x_i + \Delta x_{i-1}} \gamma_{i-1j} (P_{ij}^{n+1} - P_{i-1j}^{n+1}) + \\ & + \frac{2\Delta t(x_b - x_{i-1})}{\Delta y_j + \Delta y_{j-1}} \lambda_{ij-1} (P_{ij}^{n+1} - P_{ij-1}^{n+1}) = (x_i - x_{i-1})\tilde{v}_{ij} - \Delta y_j \tilde{u}_{i-1j} + (x_b - x_{i-1})\tilde{v}_{ij-1} \end{aligned} \quad (\text{A-10})$$

Category 5:

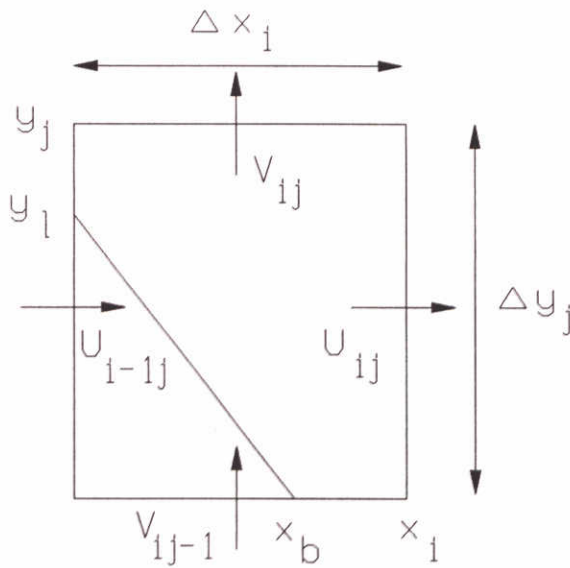


Figure A8

No virtual velocities have to be set for this category.

The mass conservation equation for this cell becomes:

$$\Delta y_j u_{ij}^{n+1} - (y_j - y_l) u_{i-1j}^{n+1} + \Delta x_i v_{ij}^{n+1} - (x_i - x_b) v_{i,j-1}^{n+1} = 0$$

From this equation and the momentum equations we can derive the pressure boundary condition for this cell:

$$\begin{aligned} & \frac{2\Delta t \Delta y_j}{\Delta x_{i+1} + \Delta x_i} \gamma_{ij} (P_{i+1j}^{n+1} - P_{ij}^{n+1}) - \frac{2\Delta t (y_j - y_l)}{\Delta x_i + \Delta x_{i-1}} \gamma_{i-1j} (P_{ij}^{n+1} - P_{i-1j}^{n+1}) + \\ & + \frac{2\Delta t \Delta x_i}{\Delta y_{j+1} + \Delta y_j} \lambda_{ij} (P_{ij+1}^{n+1} - P_{ij}^{n+1}) - \frac{2\Delta t (x_i - x_b)}{\Delta y_j + \Delta y_{j-1}} \lambda_{i,j-1} (P_{ij}^{n+1} - P_{i,j-1}^{n+1}) = \\ & \Delta y_j \tilde{u}_{ij} - (y_j - y_l) \tilde{u}_{i-1j} + \Delta x_i \tilde{v}_{ij} - (x_i - x_b) \tilde{v}_{i,j-1} \end{aligned} \quad (\text{A-11})$$

Category 6:

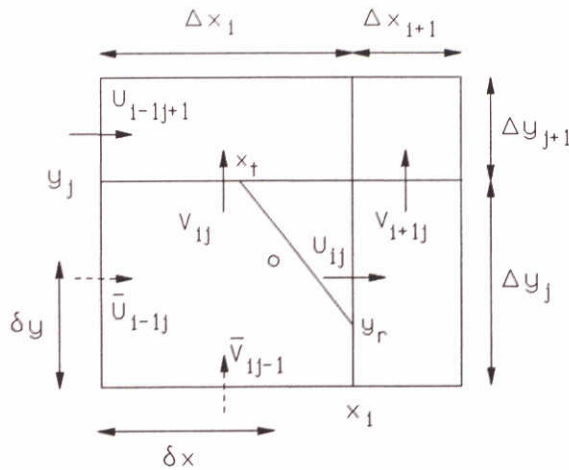


Figure A9

$$n_1 \tau_1 \left(\frac{u_{ij} - \bar{u}_{i-1j}}{\Delta x_i} - \frac{v_{ij} - \bar{v}_{ij-1}}{\Delta y_j} \right) + 2n_1 \tau_2 \frac{v_{i+1j} - v_{ij}}{\Delta x_{i+1} + \Delta x_i} + 2n_2 \tau_1 \frac{u_{i-1j+1} - \bar{u}_{i-1j}}{\Delta y_{j+1} + \Delta y_j} = 0 \quad (\text{A-12})$$

$$n_1 \left[u_{ij} + 2\left(\delta y - \frac{1}{2} \Delta y_j\right) \frac{u_{ij+1} - u_{ij}}{\Delta y_{j+1} + \Delta y_j} - (\Delta x_i - \delta x) \frac{u_{ij} - \bar{u}_{i-1j}}{\Delta x_i} \right] + \\ + n_2 \left[v_{ij} - (\Delta y_j - \delta y) \frac{v_{ij} - \bar{v}_{ij-1}}{\Delta y_j} + 2\left(\delta x - \frac{1}{2} \Delta x_i\right) \frac{v_{i+1j} - v_{ij}}{\Delta x_{i+1} + \Delta x_i} \right] = 0 \quad (\text{A-13})$$

In the program the collocation point is chosen at the centre of cell (i,j) so $\delta x = \frac{1}{2} \Delta x_i$ and $\delta y = \frac{1}{2} \Delta y_j$.

The continuity equation for this cell is:

$$(x_i - x_r) v_{ij}^{n+1} + (y_j - y_r) u_{ij}^{n+1} = 0$$

we find the pressure boundary condition:

$$\frac{2\Delta t(x_i - x_r)}{\Delta y_{j+1} + \Delta y_j} \lambda_{ij} (P_{ij+1}^{n+1} - P_{ij}^{n+1}) + \frac{2\Delta t(y_j - y_r)}{\Delta x_{i+1} + \Delta x_i} \gamma_{ij} (P_{i+1j}^{n+1} - P_{ij}^{n+1}) = \\ (x_i - x_r) \tilde{v}_{ij} + (y_j - y_r) \tilde{u}_{ij} \quad (\text{A-14})$$

Category 7:

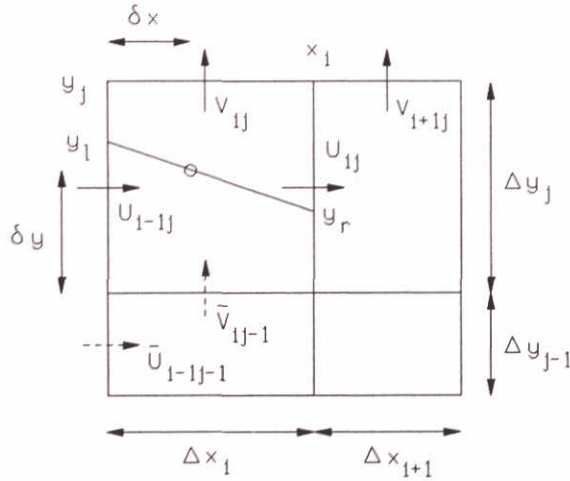


Figure A10

$$n_1 \tau_1 \left(\frac{u_{ij} - u_{i-1j}}{\Delta x_i} - \frac{v_{ij} - \bar{v}_{ij-1}}{\Delta y_j} \right) + 2n_1 \tau_2 \frac{v_{i+1j} - v_{ij}}{\Delta x_{i+1} + \Delta x_i} + 2n_2 \tau_1 \frac{u_{i-1j} - \bar{u}_{i-1j-1}}{\Delta y_j + \Delta y_{j-1}} = 0 \quad (\text{A-15})$$

$$n_1 \left[u_{ij} - (\Delta x_i - \delta x) \frac{u_{ij} - u_{i-1j}}{\Delta x_i} + 2 \left(\delta y - \frac{1}{2} \Delta y_j \right) \frac{u_{i-1j} - \bar{u}_{i-1j-1}}{\Delta y_j + \Delta y_{j-1}} \right] +$$

$$+ n_2 \left[v_{ij} - (\Delta y_j - \delta y) \frac{v_{ij} - \bar{v}_{ij-1}}{\Delta y_j} + 2 \left(\delta x - \frac{1}{2} \Delta x_i \right) \frac{v_{i+1j} - v_{ij}}{\Delta x_{i+1} + \Delta x_i} \right] = 0 \quad (\text{A-16})$$

The mass conservation equation for this cell becomes:

$$(y_j - y_r) u_{ij}^{n+1} - (y_j - y_l) u_{i-1j}^{n+1} + \Delta x_i v_{ij}^{n+1} = 0$$

The pressure boundary condition derived from this is:

$$\frac{2\Delta t(y_j - y_r)}{\Delta x_{i+1} + \Delta x_i} \gamma_{ij} (P_{i+1j}^{n+1} - P_{ij}^{n+1}) - \frac{2\Delta t(y_j - y_l)}{\Delta x_i + \Delta x_{i-1}} \gamma_{i-1j} (P_{ij}^{n+1} - P_{i-1j}^{n+1}) +$$

$$+ \frac{2\Delta t \Delta x_i}{\Delta y_{j+1} + \Delta y_j} \lambda_{ij} (P_{ij+1}^{n+1} - P_{ij}^{n+1}) = (y_j - y_r) \bar{u}_{ij} - (y_j - y_l) \bar{u}_{i-1j} + \Delta x_i \bar{v}_{ij} \quad (\text{A-17})$$

Category 8:

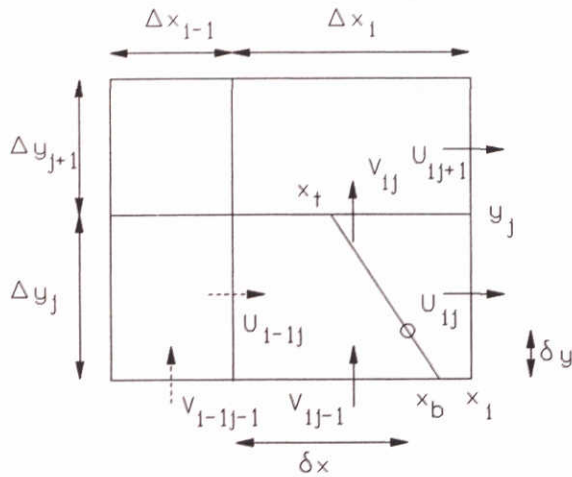


Figure A11

$$n_1 \tau_1 \left(\frac{u_{ij} - \bar{u}_{i-1j}}{\Delta x_i} - \frac{v_{ij} - v_{ij-1}}{\Delta y_j} \right) + 2n_1 \tau_2 \frac{v_{ij-1} - \bar{v}_{i-1j-1}}{\Delta x_i + \Delta x_{i-1}} + 2n_2 \tau_1 \frac{u_{ij+1} - u_{ij}}{\Delta y_{j+1} + \Delta y_j} = 0 \quad (\text{A-18})$$

$$n_1 \left[u_{ij} - (\Delta x_i - \delta x) \frac{u_{ij} - \bar{u}_{i-1j}}{\Delta x_i} + 2(\delta y - \frac{1}{2} \Delta y_j) \frac{u_{ij+1} - u_{ij}}{\Delta y_{j+1} + \Delta y_j} \right] +$$

$$+ n_2 \left[v_{ij} + 2(\delta x - \frac{1}{2} \Delta x_i) \frac{v_{ij-1} - \bar{v}_{i-1j-1}}{\Delta x_i + \Delta x_{i-1}} - (\Delta y_j - \delta y) \frac{v_{ij} - v_{ij-1}}{\Delta y_j} \right] = 0 \quad (\text{A-19})$$

Mass conservation in this cell is expressed by:

$$(x_i - x_r) v_{ij}^{n+1} - (x_i - x_b) v_{ij-1}^{n+1} + \Delta y_j u_{ij}^{n+1} = 0$$

The pressure boundary condition now becomes:

$$\frac{2\Delta t(x_i - x_r)}{\Delta y_{j+1} + \Delta y_j} \lambda_{ij} (P_{ij+1}^{n+1} - P_{ij}^{n+1}) - \frac{2\Delta t(x_i - x_b)}{\Delta y_j + \Delta y_{j-1}} \lambda_{ij-1} (P_{ij}^{n+1} - P_{ij-1}^{n+1}) +$$

$$+ \frac{2\Delta t \Delta y_j}{\Delta x_{i+1} + \Delta x_i} \gamma_{ij} (P_{i+1j}^{n+1} - P_{ij}^{n+1}) = (x_i - x_r) \tilde{v}_{ij} - (x_i - x_b) \tilde{v}_{ij-1} + \Delta y_j \tilde{u}_{ij} \quad (\text{A-20})$$

Category 9:

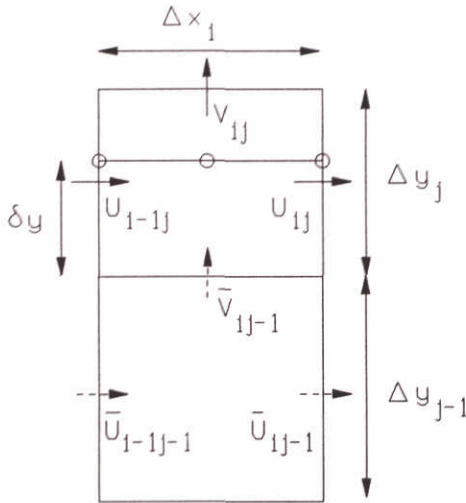


Figure A12

For horizontal and vertical surfaces the virtual velocities are not coupled. Depending on the neighbouring impermeable surface cells the free-slip condition can be used to determine a virtual velocity. The impermeability condition has to be set in all cases.

$$v_{ij} - (\Delta y_j - \delta y) \frac{v_{ij} - \bar{v}_{ij-1}}{\Delta y_j} = 0 \quad (\text{A-21})$$

$$\bar{u}_{i-1,j-1} = u_{i-1,j} \quad \text{left} \quad (\text{A-22})$$

$$\bar{u}_{ij-1} = u_{ij} \quad \text{right} \quad (\text{A-23})$$

The continuity equation for this cell becomes:

$$(u_{ij}^{n+1} - u_{i-1,j}^{n+1})(\Delta y_j - \delta y) + \Delta x_i v_{ij}^{n+1} = 0$$

from which we can derive the pressure equation at the boundary:

$$\begin{aligned} 2\Delta t \frac{\Delta y_j - \delta y}{\Delta x_i + \Delta x_{i-1}} \gamma_{i-1,j} (P_{ij}^{n+1} - P_{i-1,j}^{n+1}) - 2\Delta t \frac{\Delta y_j - \delta y}{\Delta x_{i+1} + \Delta x_i} \gamma_{i,j} (P_{i+1,j}^{n+1} - P_{ij}^{n+1}) + \\ - 2\Delta t \frac{\Delta x_i}{\Delta y_{j+1} + \Delta y_j} \lambda_{ij} (P_{ij+1}^{n+1} - P_{ij}^{n+1}) = (\bar{u}_{i-1,j} - \bar{u}_{ij})(\Delta y_j - \delta y) - \Delta x_i \bar{v}_{ij} \end{aligned} \quad (\text{A-24})$$

Category 10:

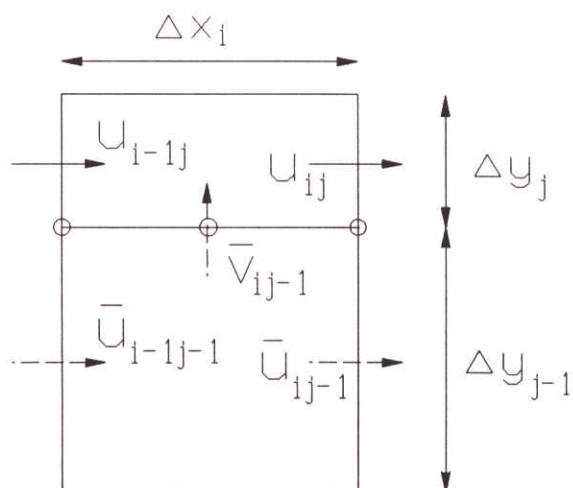


Figure A13

$$\bar{v}_{ij-1} = 0 \quad (\text{A-25})$$

$$\bar{u}_{i-1,j-1} = u_{i-1,j} \quad \text{left} \quad (\text{A-26})$$

$$\bar{u}_{ij-1} = u_{ij} \quad \text{right} \quad (\text{A-27})$$

The equation of continuity for this cell becomes:

$$\Delta y_j (u_{ij}^{n+1} - u_{i-1,j}^{n+1}) + \Delta x_i v_{ij}^{n+1} = 0$$

and the pressure boundary condition:

$$\begin{aligned} & \frac{2\Delta t \Delta y_j}{\Delta x_i + \Delta x_{i-1}} \gamma_{i-1,j} (P_{ij}^{n+1} - P_{i-1,j}^{n+1}) - \frac{2\Delta t \Delta y_j}{\Delta x_{i+1} + \Delta x_i} \gamma_{ij} (P_{i+1,j}^{n+1} - P_{ij}^{n+1}) + \\ & - \frac{2\Delta t \Delta x_i}{\Delta y_{j+1} + \Delta y_j} \lambda_{ij} (P_{ij+1}^{n+1} - P_{ij}^{n+1}) = \Delta y_j (\bar{u}_{i-1,j} - \bar{u}_{ij}) - \Delta x_i \bar{v}_{ij} \end{aligned} \quad (\text{A-28})$$

Category 11:

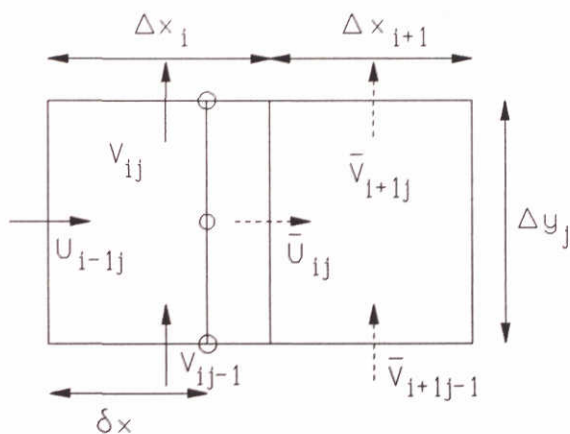


Figure A14

$$u_{i-1,j} + \delta x \frac{\bar{u}_{ij} - u_{i-1,j}}{\Delta x_i} = 0 \quad (\text{A-29})$$

$$\bar{v}_{i+1,j} = v_{ij} \quad \text{top} \quad (\text{A-30})$$

$$\bar{v}_{i+1,j-1} = v_{ij-1} \quad \text{bottom} \quad (\text{A-31})$$

From the continuity equation for this cell

$$\delta x (v_{ij}^{n+1} - v_{ij-1}^{n+1}) - \Delta y_j u_{i-1,j}^{n+1} = 0$$

we can derive the pressure boundary equation:

$$\begin{aligned} & \frac{2 \Delta t \delta x}{\Delta y_{j+1} + \Delta y_j} \lambda_{ij} (P_{ij+1}^{n+1} - P_{ij}^{n+1}) - \frac{2 \Delta t \delta x}{\Delta y_j + \Delta y_{j-1}} \lambda_{ij-1} (P_{ij}^{n+1} - P_{ij-1}^{n+1}) + \\ & - \frac{2 \Delta t \Delta y_j}{\Delta x_i + \Delta x_{i-1}} \gamma_{i-1,j} (P_{ij}^{n+1} - P_{i-1,j}^{n+1}) = \delta x (\bar{v}_{ij} - \bar{v}_{ij-1}) - \Delta y_j \bar{u}_{i-1,j} \end{aligned} \quad (\text{A-32})$$

Category 12:

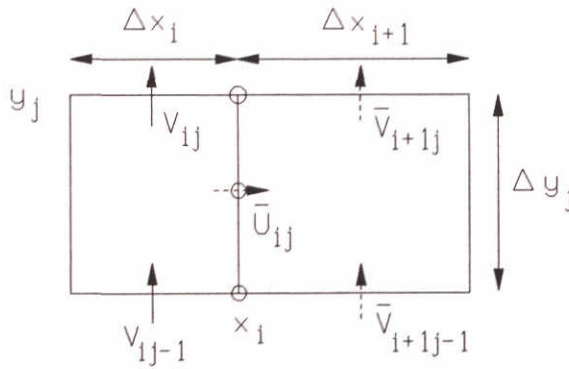


Figure A15

$$\bar{u}_{ij} = 0 \quad (\text{A-33})$$

$$\bar{v}_{i+1,j} = v_{ij} \quad \text{top} \quad (\text{A-34})$$

$$\bar{v}_{i+1,j-1} = v_{ij-1} \quad \text{bottom} \quad (\text{A-35})$$

The continuity equation for this cell is

$$\Delta x_i (v_{ij}^{n+1} - v_{ij-1}^{n+1}) - \Delta y_j (u_{i+1,j}^{n+1} - u_{i,j}^{n+1}) = 0$$

from which we find the pressure boundary equation:

$$\begin{aligned} & \frac{2 \Delta t \Delta x_i}{\Delta y_{j+1} + \Delta y_j} \lambda_{ij} (P_{ij+1}^{n+1} - P_{ij}^{n+1}) - \frac{2 \Delta t \Delta x_i}{\Delta y_j + \Delta y_{j-1}} \lambda_{ij-1} (P_{ij}^{n+1} - P_{ij-1}^{n+1}) + \\ & - \frac{2 \Delta t \Delta y_j}{\Delta x_i + \Delta x_{i-1}} \gamma_{i-1,j} (P_{ij}^{n+1} - P_{i-1,j}^{n+1}) = \Delta x_i (\tilde{v}_{ij} - \tilde{v}_{ij-1}) - \Delta y_j (\tilde{u}_{i+1,j} - \tilde{u}_{i,j}) \end{aligned} \quad (\text{A-36})$$

Category 13:

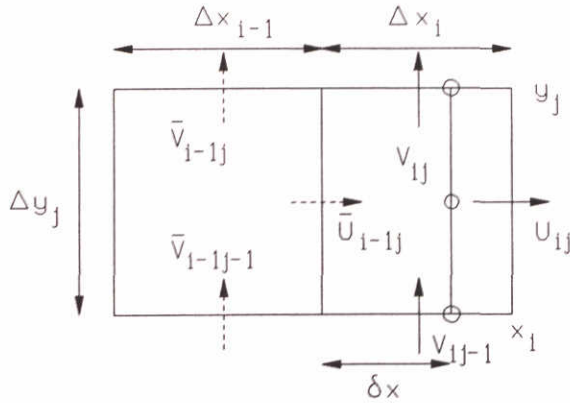


Figure A16

$$u_{ij} - (\Delta x_i - \delta x) \frac{u_{ij} - \bar{u}_{i-1/2,j}}{\Delta x_i} = 0 \quad (\text{A-37})$$

$$\bar{v}_{i-1/2,j} = v_{ij} \quad \text{top} \quad (\text{A-38})$$

$$\bar{v}_{i-1/2,j-1} = v_{ij-1} \quad \text{bottom} \quad (\text{A-39})$$

For this cell conservation of mass is expressed by:

$$(\Delta x_i - \delta x)(v_{ij}^{n+1} - v_{ij-1}^{n+1}) + \Delta y_j u_{ij}^{n+1} = 0$$

The pressure boundary condition now becomes:

$$\begin{aligned} & \frac{2\Delta t(\Delta x_i - \delta x)}{\Delta y_{j+1} + \Delta y_j} \lambda_{ij}(P_{ij+1}^{n+1} - P_{ij}^{n+1}) - \frac{2\Delta t(\Delta x_i - \delta x)}{\Delta y_j + \Delta y_{j-1}} \lambda_{ij-1}(P_{ij}^{n+1} - P_{ij-1}^{n+1}) + \\ & + \frac{2\Delta t\Delta y_j}{\Delta x_{i+1} + \Delta x_i} \gamma_{ij}(P_{i+1,j}^{n+1} - P_{ij}^{n+1}) = (\Delta x_i - \delta x)(\bar{v}_{ij} - \bar{v}_{ij-1}) + \Delta y_j \bar{u}_{ij} \end{aligned} \quad (\text{A-40})$$

Category 14:

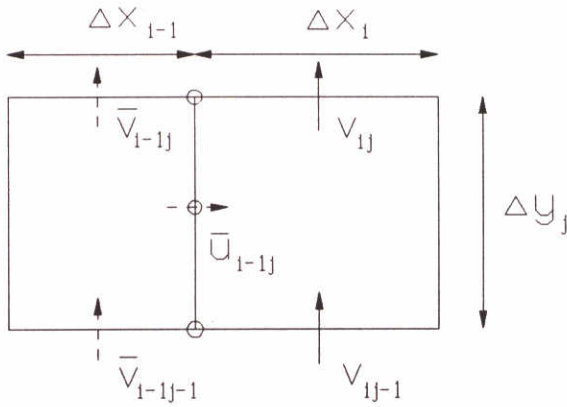


Figure A17

$$\bar{u}_{i-1,j} = 0 \quad (\text{A-41})$$

$$\bar{v}_{i-1,j} = v_{ij} \quad \text{top} \quad (\text{A-42})$$

$$\bar{v}_{i-1,j-1} = v_{ij-1} \quad \text{bottom} \quad (\text{A-43})$$

For this cell the continuity equation is:

$$\Delta x_i (v_{ij}^{n+1} - v_{ij-1}^{n+1}) + \Delta y_j (u_{ij}^{n+1} - u_{i-1,j}^{n+1}) = 0$$

The pressure boundary condition now becomes:

$$\begin{aligned} & \frac{2\Delta t \Delta x_i}{\Delta y_{j+1} + \Delta y_j} \lambda_{ij} (P_{ij+1}^{n+1} - P_{ij}^{n+1}) - \frac{2\Delta t \Delta x_i}{\Delta y_j + \Delta y_{j-1}} \lambda_{ij-1} (P_{ij}^{n+1} - P_{ij-1}^{n+1}) + \\ & + \frac{2\Delta t \Delta y_j}{\Delta x_{i+1} + \Delta x_i} \gamma_{ij} (P_{i+1,j}^{n+1} - P_{ij}^{n+1}) = \Delta x_i (\tilde{v}_{ij} - \tilde{v}_{ij-1}) + \Delta y_j \tilde{u}_{ij} \end{aligned} \quad (\text{A-A4})$$

Since in some cases where horizontal or vertical slopes are involved, virtual velocities can be defined twice (see example in Figure A18), we choose to give up the free slip condition at the end point of the horizontal or vertical slope in these cases.

In the program this could be realized by, first dealing with the categories 9 to 14, setting 3 virtual velocities for each of these cells. After that the other categories are dealt with, which results in overwriting in conflicting cases.

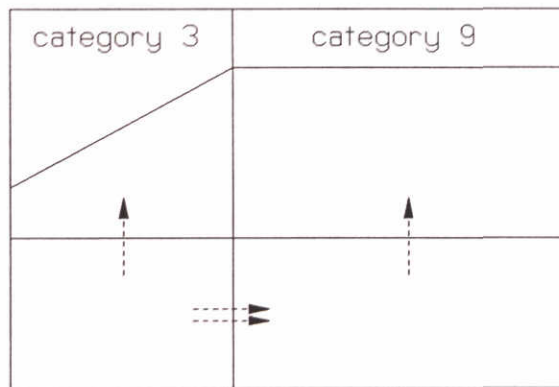


Figure A18 Conflicting boundary conditions

Treatment of surface cells at the slope

In order to set velocities at those cell interfaces which are dry and belong to a surface cell, we first try to meet the combined impermeability condition and continuity condition at the slope. At the point where the free surface and the slope meet we also need to make some adjustment in the pressure equation.

Empty cell at the *RIGHT*

Category 1:	$u_{ij} = u_{i-1j},$	$P_{ij} = 0$
Category 3:	$u_{ij} = u_{i-1j},$	$P_{ij} = P_{ij+1}$
Category 5:	$u_{ij} = u_{i-1j},$	$P_{ij} = 0$
Category 6:	$u_{ij} = \frac{x_i - x_t}{y_j - y_r} v_{ij},$	$P_{ij} = P_{ij+1}$
Category 7:	$u_{ij} = u_{i-1j},$	$P_{ij} = P_{ij+1}$
Category 8:	$u_{ij} = \frac{(x_i - x_b) v_{ij-1} - (x_i - x_t) v_{ij}}{\Delta y_j},$	$P_{ij} = 0$
Category 9:	$u_{ij} = u_{i-1j},$	$P_{ij} = P_{ij+1}$
Category 10:	$u_{ij} = u_{i-1j},$	$P_{ij} = 0$
Category 13:	$u_{ij} = -\frac{\Delta x_i - \delta x}{\Delta y_j} (v_{ij} - v_{ij-1}),$	$P_{ij} = 0$
Category 14:	$u_{ij} = -\frac{\Delta x_i}{\Delta y_j} (v_{ij} - v_{ij-1}),$	$P_{ij} = 0$

Empty cell at the TOP

Category 1:	$v_{ij} = v_{ij-1},$	$P_{ij} = P_{i-1j}$
Category 2:	$v_{ij} = \frac{y_j - y_l}{x_l - x_{i-1}} u_{i-1j},$	$P_{ij} = P_{i-1j}$
Category 3:	$v_{ij} = \frac{(y_j - y_l) u_{i-1j} - (y_j - y_r) u_{ij}}{\Delta x_i},$	$P_{ij} = P_{i-1j}$
Category 4:	$v_{ij} = v_{ij-1},$	$P_{ij} = P_{i-1j}$
Category 5:	$v_{ij} = v_{ij-1},$	$P_{ij} = P_{i+1j}$
Category 6:	$v_{ij} = -\frac{y_j - y_r}{x_i - x_l} u_{ij},$	$P_{ij} = P_{i+1j}$
Category 7:	$v_{ij} = \frac{(y_j - y_l) u_{i-1j} - (y_j - y_r) u_{ij}}{\Delta x_i},$	$P_{ij} = P_{i+1j}$
Category 8:	$v_{ij} = v_{ij-1},$	$P_{ij} = P_{i+1j}$
Category 9:	$v_{ij} = -\frac{\Delta y_j - \delta y}{\Delta x_i} (u_{ij} - u_{i-1j}),$	$P_{ij} = 0$
Category 10:	$v_{ij} = -\frac{\Delta y_j}{\Delta x_i} (u_{ij} - u_{i-1j}),$	$P_{ij} = 0$
Category 11:	$v_{ij} = v_{ij-1},$	$P_{ij} = P_{i-1j}$
Category 12:	$v_{ij} = v_{ij-1},$	$P_{ij} = P_{i-1j}$
Category 13:	$v_{ij} = v_{ij-1},$	$P_{ij} = P_{i+1j}$
Category 14:	$v_{ij} = v_{ij-1},$	$P_{ij} = P_{i+1j}$

Empty cells at the RIGHT and TOP

Category 1:	$v_{ij} = v_{ij-1},$	$u_{ij} = u_{i-1j},$	$P_{ij} = P_{i-1j}$
Category 3:	$v_{ij} = \frac{y_r - y_l}{\Delta x_i} u_{i-1j},$	$u_{ij} = u_{i-1j},$	$P_{ij} = P_{i-1j}$
Category 5:	$v_{ij} = v_{ij-1},$	$u_{ij} = u_{i-1j},$	$P_{ij} = 0$
Category 6:	$u_{ij} = 0,$	$v_{ij} = 0,$	$P_{ij} = 0$
Category 7:	$u_{ij} = u_{i-1j},$	$v_{ij} = -\frac{y_l - y_r}{\Delta x_i} u_{i-1j},$	$P_{ij} = 0$
Category 8:	$v_{ij} = v_{ij-1},$	$u_{ij} = -\frac{x_b - x_l}{\Delta y_j} v_{ij-1},$	$P_{ij} = 0$
Category 9:	$u_{ij} = u_{i-1j},$	$v_{ij} = 0,$	$P_{ij} = 0$
Category 10:	$u_{ij} = u_{i-1j},$	$v_{ij} = 0,$	$P_{ij} = 0$

$$\text{Category 13: } v_{ij} = v_{ij-1}, \quad u_{ij} = 0, \quad P_{ij} = 0$$

$$\text{Category 14: } v_{ij} = v_{ij-1}, \quad u_{ij} = 0, \quad P_{ij} = 0$$

Empty cell at the *LEFT*

$$\text{Category 1: } u_{i-1j} = u_{ij}, \quad P_{ij} = 0$$

$$\text{Category 2: } u_{i-1j} = \frac{x_i - x_{i-1}}{y_j - y_l} v_{ij}, \quad P_{ij} = P_{ij+1}$$

$$\text{Category 3: } u_{i-1j} = u_{ij}, \quad P_{ij} = P_{ij+1}$$

$$\text{Category 4: } u_{i-1j} = \frac{(x_i - x_{i-1})v_{ij} - (x_b - x_{i-1})v_{ij-1}}{\Delta y_j}, \quad P_{ij} = 0$$

$$\text{Category 5: } u_{i-1j} = u_{ij}, \quad P_{ij} = 0$$

$$\text{Category 7: } u_{i-1j} = u_{ij}, \quad P_{ij} = P_{ij+1}$$

$$\text{Category 9: } u_{i-1j} = u_{ij}, \quad P_{ij} = 0$$

$$\text{Category 10: } u_{i-1j} = u_{ij}, \quad P_{ij} = 0$$

$$\text{Category 11: } u_{i-1j} = \frac{\delta x}{\Delta y_j} (v_{ij} - v_{ij-1}), \quad P_{ij} = 0$$

$$\text{Category 12: } u_{i-1j} = \frac{\Delta x_i}{\Delta y_j} (v_{ij} - v_{ij-1}), \quad P_{ij} = 0$$

Empty cells at the *RIGHT* and *LEFT*

$$\text{Category 1: } u_{ij} = 0, \quad u_{i-1j} = 0, \quad P_{ij} = 0$$

$$\text{Category 3: } u_{ij} = 0, \quad u_{i-1j} = \frac{v_{ij} \Delta x_i}{y_j - y_l}, \quad P_{ij} = 0$$

$$\text{Category 5: } u_{ij} = 0, \quad u_{i-1j} = 0, \quad P_{ij} = 0$$

$$\text{Category 7: } u_{ij} = -\frac{v_{ij} \Delta x_i}{y_j - y_r}, \quad u_{i-1j} = 0, \quad P_{ij} = 0$$

$$\text{Category 9: } u_{ij} = -\frac{1}{2} \frac{v_{ij} \Delta x_i}{y_j - y_r}, \quad u_{i-1j} = -u_{ij}, \quad P_{ij} = 0$$

$$\text{Category 10: } u_{ij} = -\frac{v_{ij} \Delta x_i}{2 \Delta y_j}, \quad u_{i-1j} = -u_{ij}, \quad P_{ij} = 0$$

Empty cells at the TOP and LEFT

Category 1:	$v_{ij} = v_{ij-1},$	$u_{i-1j} = u_{ij},$	$p_{ij} = 0$
Category 2:	$u_{i-1j} = 0,$	$v_{ij} = 0,$	$p_{ij} = 0$
Category 3:	$v_{ij} = \frac{y_r - y_l}{\Delta x_i} u_{ij},$	$u_{i-1j} = u_{ij},$	$p_{ij} = 0$
Category 4:	$v_{ij} = v_{ij-1},$	$u_{i-1j} = \frac{(x_t - x_{i-1})v_{ij} - (x_b - x_{i-1})v_{ij-1}}{\Delta y_j},$	$p_{ij} = 0$
Category 5:	$v_{ij} = v_{ij-1},$	$u_{i-1j} = u_{ij},$	$p_{ij} = p_{i+1j}$
Category 7:	$u_{i-1j} = u_{ij},$	$v_{ij} = -\frac{y_l - y_r}{\Delta x_i} u_{ij},$	$p_{ij} = p_{i+1j}$
Category 9:	$v_{ij} = 0,$	$u_{i-1j} = u_{ij},$	$p_{ij} = 0$
Category 10:	$u_{i-1j} = u_{ij},$	$v_{ij} = 0,$	$p_{ij} = 0$
Category 11:	$v_{ij} = v_{ij-1},$	$u_{i-1j} = 0,$	$p_{ij} = 0$
Category 12:	$v_{ij} = v_{ij-1},$	$u_{i-1j} = 0,$	$p_{ij} = 0$

Empty cells at the RIGHT, LEFT and TOP

Category 1:	$u_{ij} = 0,$	$v_{ij} = v_{ij-1},$	$u_{i-1j} = 0,$	$p_{ij} = 0$
Category 3:	$u_{ij} = 0,$	$v_{ij} = 0,$	$u_{i-1j} = 0,$	$p_{ij} = 0$
Category 5:	$u_{ij} = 0,$	$v_{ij} = v_{ij-1},$	$u_{i-1j} = 0,$	$p_{ij} = 0$
Category 7:	$u_{ij} = 0,$	$v_{ij} = 0,$	$u_{i-1j} = 0,$	$p_{ij} = 0$
Category 9:	$u_{ij} = 0,$	$v_{ij} = 0,$	$u_{i-1j} = 0,$	$p_{ij} = 0$
Category 10:	$u_{ij} = 0,$	$u_{i-1j} = 0,$	$v_{ij} = 0,$	$p_{ij} = 0$

Empty cell at BOTTOM

Category 1:	$v_{ij-1} = v_{ij},$	$p_{ij} = 0$
Category 4:	$v_{ij-1} = v_{ij},$	$p_{ij} = p_{i-1j}$
Category 5:	$v_{ij-1} = v_{ij},$	$p_{ij} = 0$
Category 8:	$v_{ij-1} = v_{ij},$	$p_{ij} = p_{i+1j}$

- Category 11: $v_{ij-1} = v_{ij}$, $P_{ij} = P_{i-1j}$
- Category 12: $v_{ij-1} = v_{ij}$, $P_{ij} = P_{i-1j}$
- Category 13: $v_{ij-1} = v_{ij}$, $P_{ij} = P_{i+1j}$
- Category 14: $v_{ij-1} = v_{ij}$, $P_{ij} = 0$

Empty cells at the *RIGHT* and *BOTTOM*

- Category 1: $u_{ij} = u_{i-1j}$, $v_{ij-1} = v_{ij}$, $P_{ij} = 0$
- Category 5: $v_{ij-1} = v_{ij}$, $u_{ij} = u_{i-1j}$, $P_{ij} = 0$
- Category 8: $v_{ij-1} = v_{ij}$, $u_{ij} = -\frac{x_b - x_t}{\Delta y_j} v_{ij}$, $P_{ij} = P_{ij+1}$
- Category 13: $v_{ij-1} = v_{ij}$, $u_{ij} = 0$, $P_{ij} = 0$
- Category 14: $v_{ij-1} = v_{ij}$, $u_{ij} = 0$, $P_{ij} = 0$

Empty cells at the *TOP* and *BOTTOM*

- Category 1: $v_{ij} = 0$, $v_{ij-1} = \frac{\Delta y_j (u_{ij} - u_{i-1j})}{\Delta x_i}$, $P_{ij} = 0$
- Category 4: $v_{ij} = \frac{\Delta y_j u_{i-1j}}{x_t + x_b - 2x_{i-1}}$, $v_{ij-1} = -v_{ij}$, $P_{ij} = 0$
- Category 5: $v_{ij} = 0$, $v_{ij-1} = \frac{\Delta y_j u_{ij} - (y_j - y_l) u_{i-1j}}{x_i - x_b}$, $P_{ij} = 0$
- Category 8: $v_{ij} = \frac{-u_{ij} \Delta y_j}{2x_i - x_t - x_b}$, $v_{ij-1} = -v_{ij}$, $P_{ij} = 0$
- Category 11: $v_{ij} = \frac{u_{i-1j} \Delta y_j}{2\delta x}$, $v_{ij-1} = -v_{ij}$, $P_{ij} = 0$
- Category 12: $v_{ij} = \frac{u_{i-1j} \Delta y_j}{2\Delta x_i}$, $v_{ij-1} = -v_{ij}$, $P_{ij} = 0$
- Category 13: $v_{ij} = \frac{-u_{ij} \Delta y_j}{2(\Delta x_i - \delta x)}$, $v_{ij-1} = -v_{ij}$, $P_{ij} = 0$
- Category 14: $v_{ij} = \frac{u_{i-1j} \Delta y_j}{2\Delta x_i}$, $v_{ij-1} = -v_{ij}$, $P_{ij} = 0$

Empty cells at TOP, RIGHT and BOTTOM

Category 1:	$v_{ij}=0,$	$u_{ij}=u_{i-1j},$	$v_{ij-1}=0,$	$P_{ij}=0$
Category 5:	$v_{ij}=0,$	$u_{ij}=u_{i-1j},$	$v_{ij-1}=0,$	$P_{ij}=0$
Category 8:	$v_{ij}=0,$	$u_{ij}=0,$	$v_{ij-1}=0,$	$P_{ij}=0$
Category 13:	$v_{ij}=0,$	$u_{ij}=0,$	$v_{ij-1}=0,$	$P_{ij}=0$
Category 14:	$v_{ij}=0,$	$v_{ij-1}=0,$	$u_{ij}=0,$	$P_{ij}=0$

Empty cells at LEFT and BOTTOM

Category 1:	$v_{ij-1}=v_{ij},$	$u_{i-1j}=u_{ij},$	$P_{ij}=0$
Category 4:	$v_{ij-1}=v_{ij},$	$u_{i-1j}=\frac{x_t-x_b}{\Delta y_j}v_{ij},$	$P_{ij}=P_{ij+1}$
Category 5:	$v_{ij-1}=v_{ij},$	$u_{i-1j}=u_{ij},$	$P_{ij}=0$
Category 11:	$v_{ij-1}=v_{ij},$	$u_{i-1j}=0,$	$P_{ij}=0$
Category 12:	$v_{ij-1}=v_{ij},$	$u_{i-1j}=0,$	$P_{ij}=0$

Empty cells at LEFT, RIGHT and BOTTOM

Category 1:	$u_{i-1j}=0,$	$u_{ij}=0,$	$v_{ij-1}=v_{ij},$	$P_{ij}=0$
Category 5:	$u_{i-1j}=0,$	$u_{ij}=0,$	$v_{ij-1}=v_{ij},$	$P_{ij}=0$

Empty cells at LEFT, TOP and BOTTOM

Category 1:	$v_{ij-1}=0,$	$v_{ij}=0,$	$u_{i-1j}=u_{ij},$	$P_{ij}=0$
Category 4:	$v_{ij-1}=0,$	$v_{ij}=0,$	$u_{i-1j}=0,$	$P_{ij}=0$
Category 5:	$v_{ij-1}=0,$	$v_{ij}=0,$	$u_{i-1j}=u_{ij},$	$P_{ij}=0$
Category 11:	$v_{ij-1}=0,$	$v_{ij}=0,$	$u_{i-1j}=0,$	$P_{ij}=0$
Category 12:	$v_{ij-1}=0,$	$v_{ij}=0,$	$u_{i-1j}=0,$	$P_{ij}=0$

Empty cells at the *LEFT, RIGHT, TOP* and *BOTTOM*

Category 1: $u_{ij}=0$, $u_{i-1j}=0$, $v_{ij}=0$, $v_{ij-1}=0$, $P_{ij}=0$

Category 5: $u_{ij}=0$, $u_{i-1j}=0$, $v_{ij}=0$, $v_{ij-1}=0$, $P_{ij}=0$

Appendix B

**Suggested approach for releasing a jet of water
at an edge on the slope**

Suggested approach for releasing a jet of water at an edge on the slope

Especially in the case of overtopping waves where the horizontal velocity is large, problems can occur with the implemented boundary conditions for the impermeable slope. At the edge near the top just where the slope becomes falling the jet of overtopping water should be released from the slope. The SKYLLA boundary conditions however tend to prevent this as they just model that the velocity component in a direction normal to the boundary must be zero.

In Figure B1 we show a situation which can cause problems in SKYLLA.

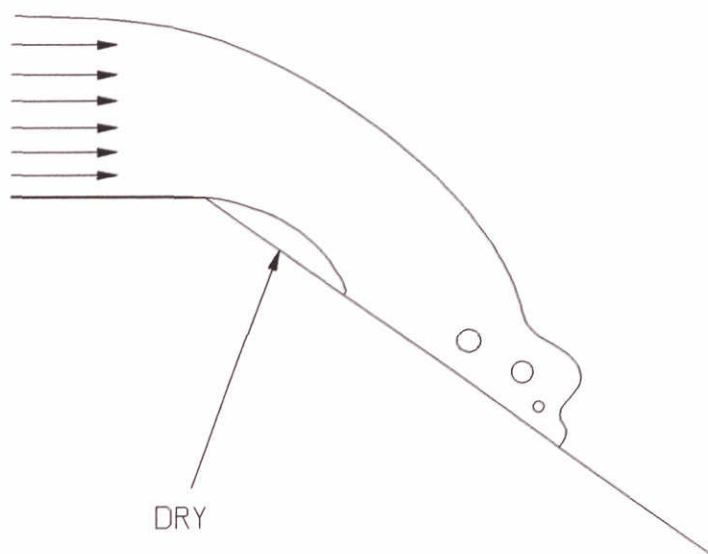


Figure B1 Overtopping jet is released from the slope

In this appendix a method is suggested to overcome the problems mentioned. This method has not been implemented in the SKYLLA code and it is only concentrated on a selection of cell categories.

We will only consider the simple case of 5 different cell categories where a jet of water should be released from or attached to the slope. For each of these cells the outgoing mass flux is one of the quantities which determine what kind of boundary condition is to be used in that particular cell. It is defined as:

$M = \oint \mathbf{u} \cdot \mathbf{n} \, dl$ where the integral is taken over the boundary of that part of the cell which can contain water.

Another quantity which is used to determine the kind of boundary condition to be used is the pressure.

If a cell at the slope does not contain water ($F=0$) but is approached by a free surface, The velocity components at the boundary of the cell are at first determined by the velocities of the free surface as soon as it is close enough. In that case the velocity components u and v are copied into the dry cell. From these velocities it can be determined whether the oncoming water is initially going to fill up the cell or not. In the situation sketched in Figure B1 this is clearly not the case for the first cell right from the top. In Figure B2 assumed copied velocities are shown for a cell of category 6A which is the first cell on the falling part of

the slope. Since we know that the horizontal velocity components will be greater than the vertical components $M > 0$ in this case. Here the cell should be treated as a free surface cell.

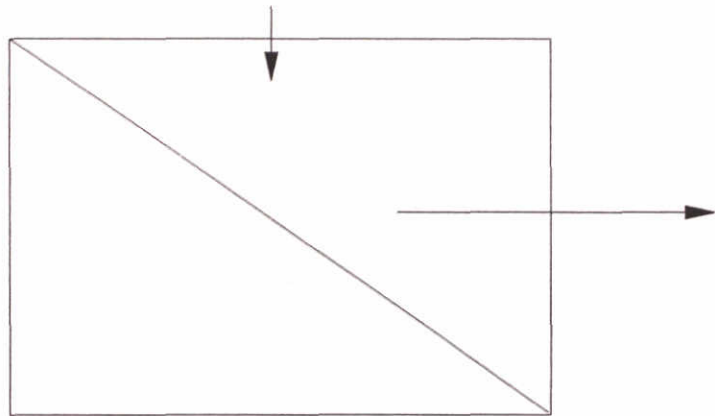


Figure B2 Copied velocities at edge

In Table B1 we show whether the cell is to be treated as a free surface cell (release) or as a cell in which the impermeability- and free slip conditions must be applied (attach).

	$M \leq -M_0$	$-M_0 \leq M \leq M_0$	$M < M_0$
$P < P_0$	attach	release	release
$P \geq P_0$	attach	attach	release

Table B1

By choosing a negative value for P_0 a flow which is in contact with the slope on both sides of the edge will not be released from the slope too easily. Taking a positive value for M_0 will prevent a jet of water, which is released from the slope at the edge, to be forced back to the slope too soon.

In the following the actions to be taken for cell categories 12, 2A, 10, 6A and 14 will be discussed for the case in which the water is to be released from the slope. Note that the F values which are set here are defined in virtual cells. Setting these values to zero guarantees that the cell where the water is released is treated as a free surface cell.

Category 12

$$M := -u_{i-1j} \Delta y_j + (v_{ij} - v_{ij-1}) \Delta x_i$$

release: $F_{i+1j} := 0$

Category 2A

$$M := -u_{i-1j} \Delta y_j + v_{ij} \Delta x_i$$

release: $u_{i-1j} < 0 \rightarrow F_{ij-1} := 0$

$$v_{ij} > 0 \rightarrow F_{i+1j} := 0$$

Category 10

$$M := (u_{ij} - u_{i-1j}) \Delta y_j + v_{ij} \Delta x_i$$

release: $F_{ij-1} := 0$

Category 6A

$$M := u_{ij} \Delta y_j + v_{ij} \Delta x_i$$

release: $u_{ij} > 0 \rightarrow F_{ij-1} := 0$

$$v_{ij} > 0 \rightarrow F_{i-1j} := 0$$

Category 14

$$M := u_{ij} \Delta y_j + (v_{ij} - v_{ij-1}) \Delta x_i$$

release: $F_{i-1j} := 0$

The actions suggested here only cope with the simple cases where the edge coincides with a grid point. The problem with the more general situation where an edge is located on the boundary of a grid cell has not been studied yet.

Appendix C

Stability considerations

Stability considerations

Internal stability considerations

A stability analysis for the discretized Navier-Stokes equations in SKYLLA is extremely difficult as the equations are nonlinear. By linearizing the equations however a simpler problem can be studied which can still provide us with conditions to determine restrictions to the time-step or space-steps. Although the conditions derived from linearized equations do not warrant stability, experience has shown that in most practical applications these kind of conditions suffice.

The model equation we study looks like:

$$\frac{\partial u}{\partial t} + \hat{u} \frac{\partial u}{\partial x} + \hat{v} \frac{\partial u}{\partial y} = \nu \left(\frac{\partial^2 u}{\partial x^2} + \frac{\partial^2 u}{\partial y^2} \right) \quad (\text{C-1})$$

Here \hat{u} and \hat{v} are the so called frozen coefficients of the equation and should be regarded as constants.

Our model equation is a special case of the problem studied by Hindmarsch et al. (1984). In their article they derive a necessary and sufficient stability criterion for the time-explicit central discretization of the advection diffusion equation in M dimensions:

$$\frac{\partial \phi}{\partial t} + \sum_{m=1}^M u_m \frac{\partial \phi}{\partial x_m} = \sum_{m=1}^M K_m \frac{\partial^2 \phi}{\partial x_m^2} \quad (\text{C-2})$$

where

$$K_m > 0 \text{ for } m = 1(1)M.$$

With the definitions $\gamma_m = K_m \Delta t / \Delta x_m^2$ and $\mu_m = u_m \Delta t / \Delta x_m$ they find after substitution of the Fourier mode $\phi_j^n = \xi^n \exp \left[i \sum_{m=1}^M j_m \theta_m \right]$ into their scheme:

$$\xi - 1 + i \sum_{m=1}^M \mu_m \sin \theta_m = \sum_{m=1}^M 2\gamma_m (\cos \theta_m - 1) \quad (\text{C-3})$$

where j is a multi-index.

The scheme is defined to be stable if $|\xi| \leq 1$ for all $\theta_m \in [0, \pi]$. They find the following

Theorem:

The central space forward time scheme for Eq.(C-2) is stable (in the von Neumann sense) if and only if:

$$\sum_{m=1}^M \gamma_m \leq \frac{1}{2} \quad (C-4)$$

and

$$\sum_{m=1}^M \frac{\mu_m^2}{\gamma_m} \leq 2. \quad (C-5)$$

When a partial upwind scheme is used which discretizes $u_m \frac{\partial \phi}{\partial x_m}$ for positive values of u_m as:

$$u_m \left(\alpha_m \frac{\phi_j - \Lambda_m^{-1} \phi_j}{\Delta x_m} + (1 - \alpha_m) \frac{\Lambda_m^1 \phi_j - \Lambda_m^{-1} \phi_j}{2 \Delta x_m} \right)$$

Equation (C-3) has to be replaced by:

$$\xi - 1 + I \sum_{m=1}^M \mu_m \sin \theta_m = \sum_{m=1}^M (2 \gamma_m + \mu_m \alpha_m) (\cos \theta_m - 1).$$

Here α_m is the upwind fraction used in the scheme in space direction m and Λ_m is a shift operator which operates on the m -th index:

$$\Lambda_m^q \phi_{j_1 j_2 \dots j_m \dots j_M} = \phi_{j_1 j_2 \dots j_m + q \dots j_M}.$$

Obviously their theorem now can now be replaced by our

Corollary:

The partial upwind scheme for Equation (C-2) is stable if and only if:

$$\sum_{m=1}^M (2 \gamma_m + \alpha_m \mu_m) \leq 1 \quad (C-6)$$

and

$$\sum_{m=1}^M \frac{\mu_m^2}{2 \gamma_m + \alpha_m \mu_m} \leq 1. \quad (C-7)$$

by setting $M=2$ the conditions for our model equations are recovered.

Free surface stability considerations

Experience in the use of SKYLLA shows that instabilities during the calculations are almost exclusively generated at the free surface.

At the free surface the same space discretizations are used as elsewhere in the fluid. Some of the velocities which are needed for these discretizations are located outside the fluid domain. The local normal vector at the free surface determines from where inside the fluid these velocities are copied. There are only four directions from where the velocities can be copied as in this operation the free surface is considered either horizontal or vertical.

In Figure C1 a situation is sketched where one of the velocities is copied from within the fluid.

The model equation is given by Eq. (C1).

We assume $\hat{v} > 0$ and $\hat{u} \geq 0$ and find with the copied value $v_{ij+1}^n := v_{ij}^n$ for the partial upwind discretization:

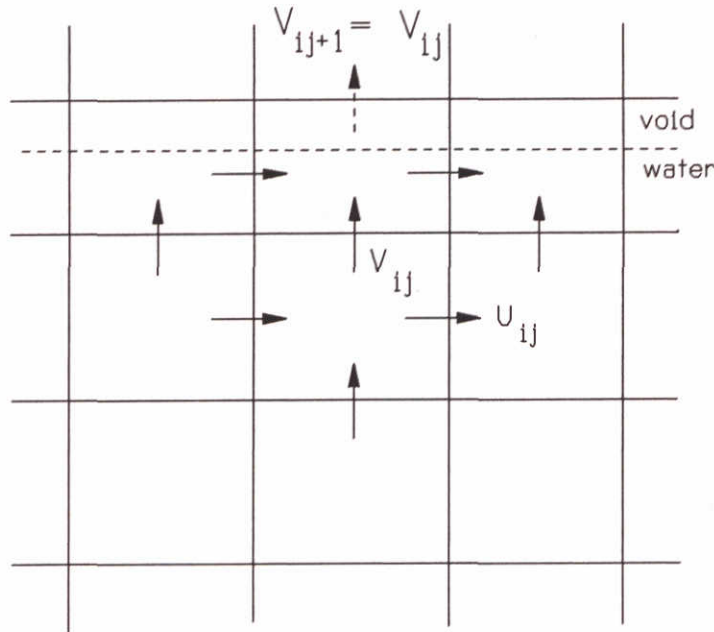


Figure C1 Fluid below the horizontal free surface

$$v_{ij}^{n+1} - v_{ij}^n + \mu_x(\alpha(v_{ij}^n - v_{i-1j}^n) + \frac{1}{2}(1 - \alpha)(v_{i+1j}^n - v_{i-1j}^n)) -$$

$$\gamma_x(v_{i+1j}^n - 2v_{ij}^n + v_{i-1j}^n) + (\frac{1}{2}(1 + \alpha)\mu_y + \gamma_y)(v_{ij}^n - v_{ij-1}^n) = 0$$

Where we use the definitions: $\mu_x := \frac{|\hat{u}| \Delta t}{\Delta x}$, $\mu_y := \frac{|\hat{v}| \Delta t}{\Delta y}$, $\gamma_x := \frac{v \Delta t}{\Delta x^2}$, $\gamma_y := \frac{v \Delta t}{\Delta y^2}$.

By substituting Fourier components $v_{ij}^n = \xi^n \exp(I\theta_x i) \exp(I\theta_y j)$, we find:

$$\xi - 1 + I\mu_x \sin \theta_x + I\left(\frac{1}{2}(1 + \alpha)\mu_y + \gamma_y\right) \sin \theta_y =$$

$$(\alpha\mu_x + 2\gamma_x)(\cos \theta_x - 1) + \left(\frac{1}{2}(1 + \alpha)\mu_y + \gamma_y\right)(\cos \theta_y - 1)$$

If we compare this equation with Eq. (C-3) and apply the theorem we find the following two stability conditions:

$$\alpha\mu_x + 2\gamma_x + \frac{1}{2}(1 + \alpha)\mu_y + \gamma_y \leq 1 \quad (\text{C-8})$$

and

$$\frac{\mu_x^2}{\alpha\mu_x + 2\gamma_x} + \frac{1}{2}(1 + \alpha)\mu_y + \gamma_y \leq 1 \quad (\text{C-9})$$

In Figure C2 we show the case where the velocity at the surface points inward. Here we have again $\hat{v} > 0$ and $\hat{u} \geq 0$ but now the velocity component v_{ij-1}^n is copied from v_{ij}^n .

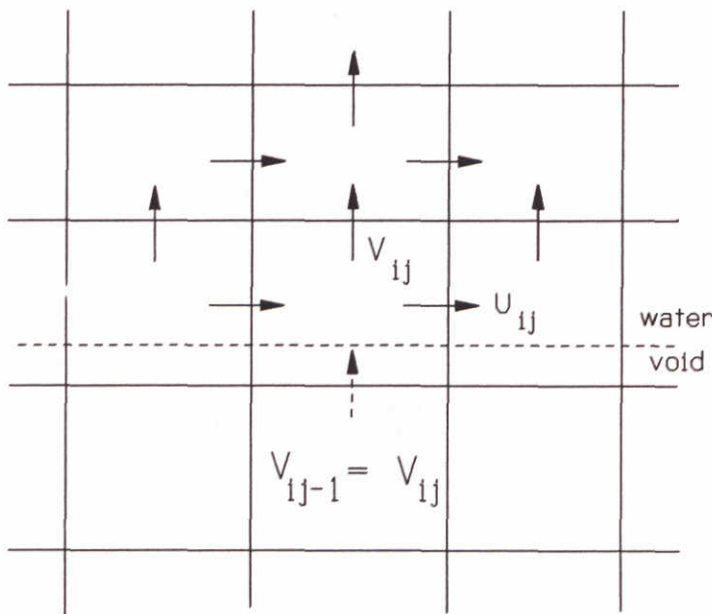


Figure C2 Fluid above the horizontal free surface

The partial upwind discretization now becomes:

$$v_{ij}^{n+1} - v_{ij}^n + \mu_x(\alpha(v_{ij}^n - v_{i-1j}^n) + \frac{1}{2}(1 - \alpha)(v_{i+1j}^n - v_{i-1j}^n))$$

$$- \gamma_x(v_{i+1j}^n - 2v_{ij}^n + v_{i-1j}^n) + \left(\frac{1}{2}(1 - \alpha)\mu_y - \gamma_y\right)(v_{ij+1}^n - v_{ij}^n) = 0 \quad (\text{C-10})$$

From the last term in this equation we can see that this is effectively a discretization of a convection term with propagation velocity $\frac{1}{2}(1-\alpha)\bar{v} - v/\Delta x$. The discretization is downwind if this value is positive and will then cause instabilities. This leads to the first of our stability conditions:

$$\gamma_y - \frac{1}{2}(1-\alpha)\mu_y \geq 0 \quad \text{or equivalently} \quad (1-\alpha)\frac{\bar{v}\Delta y}{v} \leq 2 \quad (\text{C-11})$$

Again by substitution of a Fourier component in Eq.(C-10) we find:

$$\xi - 1 + I\left(\mu_x \sin \theta_x + \left(\frac{1}{2}(1-\alpha)\mu_y - \gamma_y\right) \sin \theta_y\right) =$$

$$(\alpha \mu_x + 2\gamma_x)(\cos \theta_x - 1) + \left(\gamma_y - \frac{1}{2}(1-\alpha)\mu_y\right)(\cos \theta_y - 1)$$

By using the theorem we can now find the following two stability conditions:

$$\alpha \mu_x + 2\gamma_x + \gamma_y - \frac{1}{2}(1-\alpha)\mu_y \leq 1 \quad (\text{C-12})$$

and

$$\frac{\mu_x^2}{\alpha \mu_x + 2\gamma_x} + \gamma_y - \frac{1}{2}(1-\alpha)\mu_y \leq 1 \quad (\text{C-13})$$

For the treatment of a vertical free surface similar conditions can be derived. Conditions like in Eq. (C-11) are very unpleasant as timestep reductions can not be used to overcome the stability problems. These problems can be overcome however, by changing the upwind fraction in the discretization in these cases.

Summary of the 2D stability conditions

Here we use the definitions: $\mu_x := \frac{|\hat{u}| \Delta t}{\Delta x}$, $\mu_y := \frac{|\hat{v}| \Delta t}{\Delta y}$, $\gamma_x := \frac{v \Delta t}{\Delta x^2}$, $\gamma_y := \frac{v \Delta t}{\Delta y^2}$.

In the wet region the stability conditions become:

$$2\gamma_x + \alpha \mu_x + 2\gamma_y + \alpha \mu_y \leq 1 \quad (\text{Cs-1})$$

and

$$\frac{\mu_x^2}{2\gamma_x + \alpha \mu_x} + \frac{\mu_y^2}{2\gamma_y + \alpha \mu_y} \leq 1. \quad (\text{Cs-2})$$

At the free surface we find the following:

If the free surface is approximately horizontal there are two cases:

v1) The copied v component points toward the free surface; we now find two conditions

$$\alpha \mu_x + 2\gamma_x + \frac{1}{2}(1 + \alpha)\mu_y + \gamma_y \leq 1 \quad (\text{Cs-3})$$

and

$$\frac{\mu_x^2}{\alpha \mu_x + 2\gamma_x} + \frac{1}{2}(1 + \alpha)\mu_y + \gamma_y \leq 1 \quad (\text{Cs-4})$$

v2) The copied v component points away from the free surface; we now find three conditions

$$\gamma_y - \frac{1}{2}(1 - \alpha)\mu_y \geq 0 \quad \text{or equivalently} \quad (1 - \alpha)\frac{\tilde{v}\Delta y}{v} \leq 2, \quad (\text{Cs-5})$$

$$\alpha \mu_x + 2\gamma_x + \gamma_y - \frac{1}{2}(1 - \alpha)\mu_y \leq 1 \quad (\text{Cs-6})$$

and

$$\frac{\mu_x^2}{\alpha \mu_x + 2\gamma_x} + \gamma_y - \frac{1}{2}(1 - \alpha)\mu_y \leq 1 \quad (\text{Cs-7})$$

If the free surface is approximately vertical there are again two cases:

u1) The copied u component points toward the free surface; we now find two conditions

$$\alpha \mu_y + 2\gamma_y + \frac{1}{2}(1 + \alpha)\mu_x + \gamma_x \leq 1 \quad (\text{Cs-8})$$

and

$$\frac{\mu_y^2}{\alpha \mu_y + 2\gamma_y} + \frac{1}{2}(1 + \alpha)\mu_x + \gamma_x \leq 1 \quad (\text{Cs-9})$$

u2) The copied u component points away from the free surface; we now find three conditions

$$\gamma_x - \frac{1}{2}(1 - \alpha)\mu_x \geq 0 \quad \text{or equivalently} \quad (1 - \alpha)\frac{\tilde{u} \Delta x}{v} \leq 2, \quad (\text{Cs-10})$$

$$\alpha \mu_y + 2\gamma_y + \gamma_x - \frac{1}{2}(1 - \alpha)\mu_x \leq 1 \quad (\text{Cs-11})$$

and

$$\frac{\mu_y^2}{\alpha \mu_y + 2\gamma_y} + \gamma_x - \frac{1}{2}(1 - \alpha)\mu_x \leq 1 \quad (\text{Cs-12})$$

Problem resolving strategies

The simplest way to satisfy the stability conditions at the free surface is by setting the upwind fraction equal to 1 for those cells which have an empty neighbour. In that case we do not need to check the direction in which the free surface is moving.

The resulting 4 stability conditions with $\alpha = 1$ at the free surface then become:

$$\mu_x + 2\gamma_x + \mu_y + \gamma_y \leq 1 \quad (\text{C-14})$$

$$\mu_x + \gamma_x + \mu_y + 2\gamma_y \leq 1 \quad (\text{C-15})$$

$$\frac{\mu_x^2}{\mu_x + 2\gamma_x} + \mu_y + \gamma_y \leq 1 \quad (\text{C-16})$$

$$\mu_x + \gamma_x + \frac{\mu_y^2}{\mu_y + 2\gamma_y} \leq 1 \quad (\text{C-17})$$

Another way to solve the stability problems is found by adapting the upwind fraction in those cases where a cell-Reynolds condition is to be satisfied viz (Cs-5) and (Cs-10). In those cases the upwind fraction can be chosen to be

$$\alpha = \max(\alpha_0, 1 - \frac{2v}{|\tilde{u}| \Delta x}) \quad \text{or} \quad \alpha = \max(\alpha_0, 1 - \frac{2v}{|\tilde{v}| \Delta y})$$

respectively. This choice effectively means that the acceleration of the fluid near the free surface in the direction normal to the free surface is driven by pressure gradients and gravitational forces only in the two cases mentioned as all derivatives in the direction lateral to the free surface have been removed.

With the given choice for α only the remaining conditions need to be satisfied.

source:

'THE STABILITY OF EXPLICIT EULER TIME-INTEGRATION FOR CERTAIN FINITE DIFFERENCE APPROXIMATIONS OF THE MULTI-DIMENSIONAL ADVECTION-DIFFUSION EQUATION',
A.C.Hindmarsch, P.M.Gresho and D.F.Griffiths
International Journal for Numerical Methods in Fluids, Vol.4, pp 853-897 (1984)

Appendix D

Average-prescribing weakly-reflective boundary conditions

Average-prescribing weakly-reflective boundary conditions

The weakly-reflective boundary conditions in SKYLLA model the simple wave equation for the outgoing signals at the boundary. Where the signals are the velocity components u, v and the surface elevation η . For the surface elevation the equation becomes:

$$\frac{\partial}{\partial t}(\eta - \eta_{in}) - C \frac{\partial}{\partial x}(\eta - \eta_{in}) = 0 \quad (D-1)$$

Note that since the outgoing signal is not known it is defined as the difference between the actual signal η and the incoming signal η_{in} . For the velocity components the equations are similar. In the rest of this text we will therefore only consider the free surface elevation. The boundary condition given in Eq. (D-1) does not account for the average value of the surface elevation because only derivatives to space and time are involved. If during the calculations inaccuracies cause the average elevation to change by a constant value Eq. (D-1) is still satisfied. A remedy to this problem (suggested by G. Klopman) is found by replacing Eq. (D-1) by:

$$\frac{\partial}{\partial t}(\eta - \eta_{in}) - C \frac{\partial}{\partial x}(\eta - \eta_{in}) + r(\eta - \bar{\eta}) = 0 \quad (D-2)$$

where η_{in} is the incoming signal and $\bar{\eta}$ is the prescribed average value and r is a small value.

In order to analyze the new boundary condition we define the incoming signal:

$$\eta_{in} = \eta_0 e^{I(kx - \omega t)}$$

where ω and k satisfy the relation $C = \omega/k$ and $I^2 = -1$.

By introducing the function $A(x, t) = \eta(x, t) - \eta_{in}(x, t)$, we can write Eq.(D-2) as:

$$\frac{\partial A}{\partial t} - C \frac{\partial A}{\partial x} + rA = r(\bar{\eta} - \eta_0 e^{I(kx - \omega t)}) \quad (D-3)$$

By transforming Eq.(D-3) to the new coordinates,

$$\xi = x + Ct$$

$$\tau = t$$

we find:

$$\frac{\partial \hat{A}}{\partial \tau} + r\hat{A} = r(\bar{\eta} - \eta_0 e^{I(k\xi - 2\omega\tau)}) \quad (D-4)$$

Here we renamed $\hat{A}(\xi, \tau) \equiv A(x, t)$.

The solution of the homogeneous problem suggests a solution of the form:

$$\hat{A} = D(\xi, \tau) e^{-r\tau}.$$

By substitution in Eq.(D-4) we find the differential equation:

$$\frac{\partial D}{\partial \tau} = r e^{r\tau} (\bar{\eta} - \eta_0 e^{I(k\xi - 2\omega\tau)}).$$

Integrating to τ yields:

$$D(\xi, \tau) = \left[\bar{\eta} - \eta_0 \frac{r(r+2I\omega)}{r^2+4\omega^2} e^{I(k\xi - 2\omega\tau)} \right] e^{r\tau} + f(\xi)$$

which immediately leads to the solution of Eq.(D-4):

$$\hat{A}(\xi, \tau) = \bar{\eta} - \eta_0 \frac{r(r+2I\omega)}{r^2+4\omega^2} e^{I(k\xi - 2\omega\tau)} + f(\xi) e^{-r\tau}$$

By transforming back to the coordinates x and t we find:

$$\eta(x, t) = \bar{\eta} + \eta_0 \left(1 - \frac{r(r+2I\omega)}{r^2+4\omega^2} \right) e^{I(kx - \omega t)} + f(x + Ct) e^{-rt} \quad (D-5)$$

In the case of an initial value problem where we start with the solution:

$$\eta(x, 0) = \bar{\eta}$$

we can find by substitution in Eq.(D-5) that the solution becomes:

$$\eta(x, t) = \bar{\eta} + \eta_0 \frac{2\omega(2\omega - Ir)}{r^2+4\omega^2} (e^{I(kx - \omega t)} - e^{-rt} e^{I(kx + \omega t)}).$$

For the asymptotic behaviour of this solution we find:

$$\eta(x, t) \sim \eta_{\infty}(x, t) = \bar{\eta} + \eta_0 \frac{2\omega(2\omega - Ir)}{r^2+4\omega^2} e^{I(kx - \omega t)} \quad \text{for } t \rightarrow \infty.$$

After some manipulations we get:

$$\eta_{\infty}(x, t) = \bar{\eta} + \frac{1}{\sqrt{\left(\frac{r}{2\omega}\right)^2 + 1}} \eta_0 e^{I(kx - \omega t - \arctan(\frac{r}{2\omega}))}$$

We can conclude that the average (in time or space) indeed has the prescribed value $\bar{\eta}$. The incoming signal has been distorted however.

With the choice $\frac{r}{2\omega} = 0.1$ we find for the multiplication factor:

$$\frac{1}{\sqrt{\left(\frac{r}{2\omega}\right)^2 + 1}} = 0.995 \quad (\text{D-6})$$

and for the phase shift:

$$\arctan\left(\frac{r}{2\omega}\right) = 0.0996 \text{ rad} = 5.71^\circ \quad (\text{D-7})$$

Stability analysis

For the analysis of the upwind scheme to be used at the boundary to discretize equation (D-2) we take the homogeneous equation:

$$\frac{\partial A}{\partial t} + C \frac{\partial A}{\partial x} + rA = 0. \quad (\text{D-8})$$

Both C and r are assumed to be positive in this equation.

Note that this is the homogeneous version of equation (D-3) where for reasons of simplicity the $-C$ has been replaced by $+C$.

The upwind scheme at the boundary becomes

$$A_j^{q+1} - A_j^q + \mu (A_j^q - A_{j-1}^q) + \lambda A_j^q = 0 \quad (\text{D-9})$$

where we used the abbreviations

$$\mu = \frac{C \Delta t}{\Delta x} \text{ and } \lambda = r \Delta t.$$

By substituting a Fourier coefficient $A_j^q = \xi^q \exp(ikj\Delta x)$ in Eq. (D-9) we find

$$\xi = 1 - \lambda - \mu(1 - \cos \alpha) - i\mu \sin \alpha \quad (\text{D-10})$$

where $\alpha = k\Delta x$.

Stability in the Neumann sense is defined by $|\xi| \leq 1 \quad \forall \alpha \in [0, \frac{\pi}{2}]$.

Since $\cos \alpha$ takes all values in the interval $[-1, 1]$ for $\alpha \in [0, \frac{\pi}{2}]$ the stability condition becomes after some manipulations on Eq. (D-10):

$$((\lambda + \mu - 1)^2 + \mu^2 - 1) - 2\mu(\lambda + \mu - 1)c \leq 0 \quad \forall c \in [-1, 1].$$

From this two conditions can be derived:

$$\lambda(\lambda - 2) \leq 0$$

$$(\lambda + 2\mu)(\lambda + 2\mu - 2) \leq 0$$

As both λ and μ are positive these conditions can be reduced to only one condition which is both necessary and sufficient for stability: $\lambda + 2\mu \leq 2$

The expression for the time step now becomes:

$$\Delta t \leq \frac{2}{r+2} \frac{C}{\Delta x}$$



main office
Rotterdamseweg 185
p.o. box 177
2600 MH Delft
The Netherlands
telephone (31) 15 - 56 93 53
telefax (31) 15 - 61 96 74
telex 38176 hydel-nl

location 'De Voorst'
Voorsterweg 28, Marknesse
p.o. box 152
8300 AD Emmeloord
The Netherlands
telephone (31) 5274 - 29 22
telefax (31) 5274 - 35 73
telex 42290 hylvo-nl

